INTERNATIONAL JOURNAL OF HYDROGEN ENERGY 37 (2012) 13895–13913

Available online at www.sciencedirect.com

SciVerse ScienceDirect

journal homepage: www.elsevier.com/locate/he

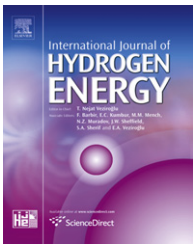

New multi-physics approach for modelling and design of alkaline electrolyzers

M. Hammoudi, C. Henao, K. Agbossou, Y. Dubé, M.L. Doumbia*

Hydrogen Research Institute, Université du Québec à Trois-Rivières, Trois-Rivières, Canada G9A5H7

ARTICLE INFO

Article history:
Received 29 March 2012
Received in revised form
4 June 2012
Accepted 4 July 2012
Available online 1 August 2012

Keywords:
Alkaline electrolyzer
Hydrogen production
High-pressure hydrogen
Bubble coverage, Multi-physic modelling
System simulation

ABSTRACT

This work presents a multi-physics model used for the design and diagnosis of the alkaline electrolyzers. The model is based on a new approach that allows to choose precisely the design parameters of a new electrolyzer even if it is not commercially available and predicting energy consumption, efficiency and rate of hydrogen production, taking into account to their physical state and various operating conditions. The approach differs from those of conventional models of the following: It allows the characterization of the electrolyzer based on its structural parameters in a relatively short time (few minutes) compared with the conventional approach which need experimental data collected for few weeks (Ulleberg). The approach allows describing a range of alkaline electrolyzers, while semi-empirical models found in literature are inherent to a specific electrolyzer. In addition, the model takes into account the variation of all structural parameters (geometry, materials and their evolution depending on operating conditions) and operational parameters of the electrolyzer (temperature, pressure, concentration, bulk bubbling and recovery rate of electrode surface by the bubble), while the models in the literature involve only the temperature. The developed multi-physics model was programmed in a Matlab Simulink® environment and an alkaline electrolyzer's simulation tool was developed. The simulation tool was validated using two industrial (Stuart and Phoebus) electrolyzers with different structures and power rates. Simulation results reproduced experimental data with good accuracy (less than 0.9%). The simulation tool was also used to compare the energy efficiency of two hydrogen production systems. The first one is based on atmospheric electrolyzer with a compressor for hydrogen storage and the second one is a barometric electrolyzer (under pressure) with its auxiliary devices to identify the effective mode of hydrogen production according to the physical state and operating conditions of the electrolyzer. The analysis of results revealed that the second mode of hydrogen production is more efficient and confirms the results of the literature based solely on the thermodynamic approach (K. Onda et al) without the input of the power consumed by power overvoltages.

* *Corresponding author.*
E-mail address: Kodjo.agbossou@uqtr.ca (K. Agbossou).

0360-3199/$ – see front matter
http://dx.doi.org/10.1016/j.ijhydene.2012.07.015

1. Introduction

1.1. Background

Electrolysis represents only 4% of world hydrogen production, because of its high cost and poor overall energy performance [1]. In a conceptual distributed energy production, conversion, storage and use system for remote communities, water electrolysis may play a significant role in this system as it produces hydrogen using renewable energy as a fuel gas for heating applications and as an energy storage mechanism. When abundant renewable energy is available, excessive energy may be stored in the form of hydrogen by water electrolysis. Different technologies are present in the market, the alkaline electrolysis is the most economically and technically mature, follows PEM technology that offers greater current density and quality of hydrogen but is restricted to low production rate not exceeding 30 Nm^3/h. SOEC technology combines the qualities of the other two types of electrolyzers but remains to this day the development stage. Nowadays, the alkaline electrolyzer remains the best alternative offering production rates ranging from 1 to 760 Nm^3/h [2] with an acceptable manufacturing cost when compared with other types of electrolyzers. This may promote its use in connected centralized or distributed production in remote sites. The scientific community estimates more or less correctly the electrolyzer power consumption by modelling the operating voltage as a function of current density and gradually introducing the parameters that affect its behaviour. In order to achieve a better estimation of power consumption and amount of hydrogen production according to physical state of the electrolyzer powered by intermittent source of energy a multi-physics model of the cell voltage is proposed in this work. The model permits to estimate exactly the power consumed by the electrolyzer, according to its physical state which is governed by different phenomena related to electrochemistry, thermodynamics and two-phase flow fluids mechanics. The new model taking into account these phenomena is aimed firstly to understand the behaviour of electrolyzers and also to optimize its management depending on its physical condition such as temperature, pressure, concentration of electrolyte, bubbling rate…. In addition, it will be a design tool, diagnostic and dimensioning of production systems based on electrolysis.

1.2. Research and development needs

Currently, the alkaline electrolyzers are commercially available and operating under temperatures between 80 and 90 °C. For higher operating temperatures, the Advanced Alkaline Electrolysis is used. "Advanced alkaline water electrolysis" was further developed in the world between the late 1970s until the mid-1980s. This transition was needed to improve the performance of the electrolyzer by increasing the operating temperature. The increasing of electrolyzer's temperature cell induces a decreasing of theoretical energy of water electrolysis ΔG and all overvoltage due to the irreversibility phenomena. High pressure and concentration of KOH (around 50%) are necessary to increase the electrolyte temperature above 100 °C in liquid phase. In this case, an important issue was the materials that resisted both high temperature and alkaline electrolyte concentration. New materials were studied by introducing an innovative pair of catalyst-electrode and cell designs by reducing the distance between electrode and a diaphragm and communally named as (zero gap). This last was generally made by asbestos and recently was substituted by potassium titanate and polyantimonic acid in order to decrease the cell resistivity LeRoy [3].

Many companies were involved in R & D on improving different components constituting the electrolyzer such as, electrode, diaphragm materials, nature of electrolytes, operating conditions, and total cell concept to lower total cell voltage and to increase current density. Operating temperature was set mainly on 80–200 °C and operating pressure is between 1 and 30 bar. In the case of atmospheric electrolyzers, a compressor unit is required to store the hydrogen produced. Operation at higher pressure would overcome the compression step and increase overall efficiency. Target of current density was 1 A/cm^2. The hydrogen production by electrolysis, induce two-phase flow phenomena in the bulk electrolyte and vicinity of electrode. The hydrogen molecules accumulate on the surface of the electrode until a bubble forms, breaks away, and rises to the surface of the electrolyte. These bubbles increase the resistance of the electrolyte and induce additional activation overvoltage due to the bubble curtain on the electrode surface [4–7]. These effects can be reduced by using an appropriate geometry of the cells (zero gap, or sandwich) and extracting more gas produced in each compartment [8].

Nowadays, reduction of cell voltage and increase of current density at operating temperature below 100 °C, by improvement of electrodes became the main targets [9]. Energy efficiency of electrolyzer including annexes systems is in the range of from 62 to 74% and the estimated operating lifetime is between 15 and 25 years.

1.3. Modelling review

In the literature, it is quite easy to find empirical models describing the evolution of the electrolyzer with its characteristic curve (current, voltage). Linear models with two parameters where the cell voltage is described by a linear function of the current are generally used to describe the steady state or stationary comportment of electrolyzer [10–12]. Note that this approximately approach often doesn't take into account the physical state of the electrolyzer (temperature, pressure, bubbling, concentration…) and therefore can not estimate correctly its energy consumption and hydrogen production capacities in transient regimes. The control of an electrolyzer described by this approach is fairly accurate and sometimes requires ballast loads with power equivalent to the electrolyzer in order to dissipate the excess energy [13]. A first improvement of the linear model was to introduce temperature-dependent parameters [14] to describe the production of hydrogen with a fairly good approximation for the electrolyzer power around 100 kW to electrolyte temperature close to 80 °C. A more realistic approach was undertaken in the early 90s with the work of Refs. [15–17] by adding to the linear equation a logarithmic term taking into account the electrochemical effects in the electrodes and with four parameters depending on temperature. This semi-

empirical correlation described more satisfactorily the evolution of the voltage at low current density compared with the linear model. Based on this same approach Ulleberg [18,19] proposed a similar approach by replacing the parameters described by affine functions of temperature with nonlinear functions of temperature. Thus, the number of parameters to be determined experimentally increases from 4 to 8. This approach remains the most useful and it reflects global changes in characteristics curve (voltage, current). Reliable determination of parameter values requires a large number of experiments to 317 [19] spanning a few weeks of work.

Most of the models [16,19] describing the electrolyzer's operating voltage are empirical requiring several sets of measurements to extract the correlation parameters describing specifically the studied electrolyzer and can not be used for another one. This mathematical approach to the problem, although based on some physical effects is not exhaustive and the majority of the models depends only on the temperature as the operating parameters, thus neglecting the impact of other parameters variation such as pressure, electrolyte concentration or bubbling rate in the bulk electrolyte and on the electrode surface. Although the empirical approach is practical, it does not identify distinctively the effects modifying the behaviour of the electrolyzer by grouping them in mathematical correlated terms. In addition, it requires the purchase of the electrolyzer to characterize and extract its curves of energy consumption and production according to its different physical states modified by the intermittent power source available to it in the case of renewable energy. Empirical modelling may represent a still image of the state of an electrolyzer for the duration of the characterization and changes during its running time are not taken into account. Likewise the change in other operating parameters such as pressure, electrolyte concentration or bubbling rate for example is not taken into account and reveals the limitations of this approach. The performance of the model depends on the accuracy and number of measurements needed to establish the mathematical correlation.

1.4. *General consideration of the new approach*

A multi-physics modelling based on identification of phenomena observed during the electrolysis allows a better understanding of the causes leading to dysfunctions of the electrolyzer and identify appropriate solutions to be made to optimize its operation. Moreover, multi-physics model would contribute to a better dimensioning of the electrolyzer given the diversity of operating conditions observed when it is fed by an intermittent renewable energy source like solar or wind. In addition, it will be a general and versatile approach describing all the alkaline electrolyzer based strictly on its static characteristics such as its size and nature of its components (electrodes, membrane and cell gap) and its operating parameters such as temperature, pressure, concentration, current density and the corresponding bubbling rate. In this context, the work presented in this paper on the multi-physics modelling of operating voltage is important by taking into account the different effects and including the operating parameters. The approach will provide a more reliable and accurate dimensioning tool thereby improving the design of systems based on hydrogen production by electrolysis alkaline. It will be the keystone of a control strategy for managing the hydrogen production and energy consumption according to the physical state of the electrolyzer powered by an intermittent power. The approach adopted in this work is more general and takes into account the thermodynamic effects, electrochemical, geometrical and two-phase flow phenomena. The latter captures the effects of flow of gas bubbles produced near the electrodes and within the electrolyte whose conductivity and viscosity are strongly affected by the gas phase. The effects of temperature, pressure and concentration were discussed in order to identify their impact on the power consumed by the electrolyzer, the thermal efficiency and the rate of hydrogen production. The model proposed uses general correlations of the electrical conductivity of the electrolyte as function of the KOH concentration and temperature and concentration and evolution of the resistivity of materials used (electrode and membrane) according to the temperature. These last are independent from the type of electrolyzer and provide from electrochemical studies of materials. Thermodynamic state variables such as enthalpy (H), entropy (S) and Gibbs free energy (G) were correlated using the tables provided from NIST and JANAF and then compared with correlations found in the literature [20–22].

2. Fundamentals of multi-physics approach for alkaline water electrolysis

2.1. *Principle of the alkaline electrolysis*

The decomposition of water into hydrogen and oxygen can be obtained by passing a direct electric current (DC) between two electrodes separated by a membrane and containing an aqueous electrolyte with good ionic conductivity. The electrodes are immersed in an alkaline aqueous solution with weight concentration (wt%) and therefore they must be corrosion resistant, have good electrical conductivity and catalytic properties, allowing better electrochemical transfer. The membrane or diaphragm separating the anode and cathode compartments is made generally with Asbestos or nickel oxide (NiO) and must have a low electrical resistance, good mechanical behaviour and low gas crossover. Usually, the anodes are made from nickel, cobalt and iron (Ni, Co, Fe), while the cathodes are made of nickel with a platinum catalyst activated carbon (Ni, Pt–C) (see Fig. 1).

A complete description of alkaline electrolysis requests a multi-physics approach including interconnecting domains such as thermodynamic, electrochemical, conceptual materials and two-phase fluid flow. For this purpose, a theoretical basis including new developments is necessary for a better comprehension of the influent effect and the implementation of the new model. The model describes the behaviour of the electrolyzer and its performance depends on fixed parameters (geometry, surface materials, pressure) and other variables parameters (concentration, electrical conductivity, bubbling).

2.2. *Thermodynamic effect*

The thermodynamic approach provides a framework for describing the equilibrium reactions according to thermal and barometric effects in electrochemical cells. It also provides a basis for defining the driving forces for transport

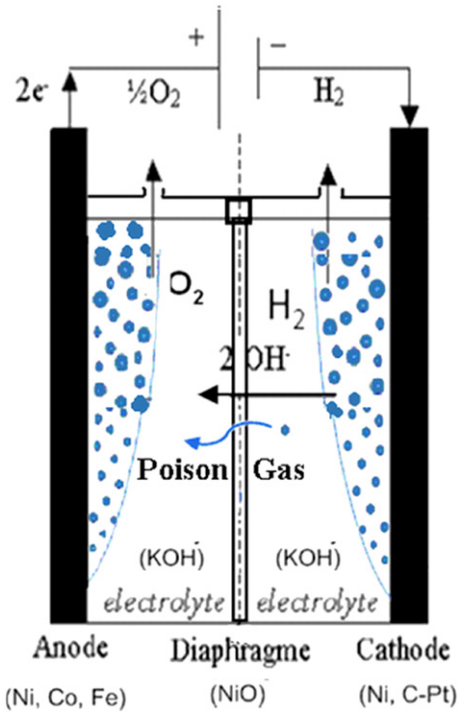

Fig. 1 – Schematic of an electrolytic cell.

phenomena in electrolytes and led to the description of the properties of electrolyte solutions [20–22].

In examining the thermodynamics of the electrolytic process, it is convenient to consider wet gases (hydrogen and oxygen) in contact with reversible electrodes containing water vapour in equilibrium with the water in the KOH solution at total pressure P and temperature T [20]. Under these conditions we assume that the partial pressure of the water vapour in each of the wet gases is equal to Pw, the aqueous vapour pressure of the KOH solution. Thus $P = Pw + P_{H_2} = Pw + P_{O_2}$.

Electrolyzer's cell voltages at operating constant pressure P and temperature T are related to thermal energy and high heating-value quantities by the amount of electricity transferred $nF = 192{,}973$ C/mol, where $(n = 2)$ denotes the number of electrons transferred and F is the Faraday constant. The total energy is expressed as a thermoneutral voltage $V_{t,P}^{tn}$ and is related to the high heating-value voltage $V_{t,P}^{HHV}$ by:

$$\Delta H_{t,P} = nFV_{t,P}^{tn} = nFV_{t,P-Pw}^{HHV} + \varphi\left(H_{t,Pw}^{w(g)} - H_{t_0,P_0}^{w(l)}\right) \quad (1)$$

where

$$\varphi = 1.5\frac{Pw}{P - Pw} \quad (2)$$

It's clear that the thermoneutral voltage $V_{t,P}^{tn}$ depends strongly on the temperature and the operating pressure.

The high heating voltage can be expressed as

$$V_{t,P}^{HHV} = V_{t,P-Pw}^{tp} + \frac{\left(H_{t,P}^{w(l)} - H_{t_0,P_0}^{w(l)}\right)}{nF} \quad (3)$$

The temperature variation of the enthalpy of formation of the liquid water at atmospheric pressure according to NIST thermophysical experimental data [23] can be correlated with relative deviation under 0.04% as:

$$-\Delta H_{f,t,P_0}^{w(l)} = nFV_{t,P_0}^{tp} = 290{,}120 - 0.048243T^2 \quad (\mathrm{J/mol}) \quad (4)$$

Note that the type of correlation proposed is different from that commonly used in the literature and proposed by LeRoy and Bowen [20] as a second-order polynomial form. This approach will get rid of the logarithmic term in the reversible potential as shown later, while the approach proposed in this work induce a second-order polynomial expression of the reversible voltage which is most convenient and more accurate than the commonly used expression in literature [20].

Thus the corresponding temperature variation of the enthalpic voltage at 1 atm can be expressed with relative deviation from NIST experimental data [23] less than 0.04%:

$$V_{T,P_0}^{tp} = 1.50342 - 2.5 \times 10^{-7}T^2 \quad (5)$$

In the case where the operating pressure increases at constant temperature, the fraction of vapour water (Pw/P) decrease and thus $P - Pw \approx P$ and $\varphi \to 0$, thus $\lim_{P\to\infty} V_{t,P}^{tn} = V_{t,P}^{HHV}$.

2.2.1. *The effect of temperature and pressure on the high heating and thermoneutral voltages*

LeRoy [20] explains the thermodynamics of water electrolysis and split the variation in temperature and barometric effects in the enthalpy equation as follows:

$$\Delta H_{t,P} - \Delta H_{t_0,P_0} = \left(\Delta H_{t,P_0} - \Delta H_{t_0,P_0}\right) + \left(\Delta H_{t,P} - \Delta H_{t,P_0}\right) \quad (6)$$

where the first term describes the thermal evolution while the second one describes the barometric evolution. Taking into account this approach, the high heating voltage can be expressed as:

$$V_{t,P}^{HHV} = V_{t,P_0}^{HHV} + f_{HHV}(T,P) \quad (7)$$

where:

$$V_{t,P_0}^{HHV} = 1.4756 + 2.252 \times 10^{-4}t + 1.52 \times 10^{-8}t^2 \quad (8)$$

Eq. (8) represents the thermal evolution of the high heating voltage at atmospheric pressure P_0 [20].

The influence of pressure can be described by the following function:

$$f_{HHV}(T,P) = \frac{\left(H_{t,P}^{H_2} - H_{t,P_0}^{H_2}\right) + 0.5\left(H_{t,P}^{O_2} - H_{t,P_0}^{O_2}\right)}{nF} = \frac{1}{nF}\int_{P_0}^{P}\left(\left(v - T\frac{\partial v}{\partial T}\right)^{H_2} + 0.5\left(v - T\frac{\partial v}{\partial T}\right)^{O_2}\right)dp \quad (9)$$

By applying the non ideal gas comportment of the hydrogen and oxygen and taking into account the modified virial equation according to the pressure, Eq. (9) becomes:

$$f_{HHV}(T,P) = \frac{1}{nF}\left(B^{H_2} + 0.5B^{O_2} - T\frac{\partial\left(B^{H_2} + 0.5B^{O_2}\right)}{\partial T}\right)P + \frac{1}{nFRT}\left[\left(C^{H_2} + 0.5C^{O_2} - \left(B^{H_2}\right)^2 - 0.5\left(B^{O_2}\right)^2 - 0.5T\left(\frac{\partial\left(C^{H_2} + 0.5C^{O_2}\right)}{\partial T} - 2\left(B^{H_2} + 0.5B^{O_2}\right)\frac{\partial\left(B^{H_2} + 0.5B^{O_2}\right)}{\partial T}\right)\right)P^2 + \cdots\right] \quad (10a)$$

where B and C are respectively the 2nd and 3rd virial coefficient of element varying with the temperature according to [20,21] and presented in Table 1:

By including the thermal evolution of the virial coefficient (Table 1) the impact of real gas considerations Eq. (10-a) can be expressed as:

$$f_{HHV}(T,P)/V=\left(21.661\times10^{-6}-\frac{10.941\times10^{-3}}{T}\right)P+\left(-\frac{18.578\times10^{-6}}{T}+\frac{0.339\times10^{-3}}{T^{1.5}}+\frac{7.845\times10^{-3}}{T^{2}}-\frac{1.659}{T^{3}}\right)P^{2} \quad (10b)$$

where the operating pressure P is expressed in bar.

The $f_{HHV}(T,P)$ term takes into account the difference voltage between ideal gas assumption and real gas considerations as precise above.

The thermoneutral voltage depends strongly on the pressure and can be expressed as according to Eq. (1):

$$V_{t,P}^{tn}=V_{t,P_0}^{HHV}+\frac{\varphi}{nF}\left(H_{t,Pw}^{w(g)}-H_{t_0,P_0}^{w(l)}\right)+f_{HHV}(T,P) \quad (11)$$

where the variation of the enthalpy of water from the liquid phase at 25 °C and 1 atm to it's value at a temperature t and pressure Pw in the gaseous phase can be expressed as function of temperature:

$$\left(H_{t,Pw}^{w(g)}-H_{t_0,P_0}^{w(l)}\right)=Y=42,960+40.762t-0.06682t^{2} \quad (12)$$

The first term of Eq. (11) represents the thermal variation of the thermoneutral voltage, the second term expresses the impact of the operating pressure and the last term express the impact of the real gas consideration on the thermoneutral voltage and will be in the same order of magnitude to the second term for operating pressure larger than 20 bar at 25 °C and higher than 120 bar at 80 °C. The second term is more important than the third one for low operating pressure and the ideal gas assumption is still justified up to 200 bar where the impact of the third term doesn't exceed 2 mV. For high operating pressure (700 bar) this value is bellow 6 mV. This investigation reveals that the thermoneutral voltage tends to the high heating voltage over operating pressure ranging from 20 to 120 bar according respectively for operating temperature ranging from 25 to 80 °C and the deviation between V_{tn} and V_{HHV} not exceed 10 mV. The difference between the two potentials is even more important as we get closer to atmospheric operating pressure.

2.2.2. The reversible potential

As part of the development of expressions for $V_{t,P}^{tp}$, $V_{t,P}^{HHV}$ and $V_{t,P}^{tn}$ it is convenient to consider an imaginary electrolytic cell under temperature and pressure conditions. The cell includes reversible electrodes in contact with wet gas. The electro motive force (emf) of such a cell would tell reversible potential, $E_{t,P}^{Rev}$ given by:

$$nFE_{t,P}^{Rev}=-\Delta G_{t,P}=\mu_{t,P}^{H_2}+0.5\mu_{t,P}^{O_2}-\mu_{t,P}^{w(g)} \quad (13)$$

In which $\mu_{t,P}^{H_2}$ is the chemical potential of hydrogen in the gaseous solution of hydrogen and water vapour, $\mu_{t,P}^{O_2}$ is the chemical potential of oxygen in the gaseous solution of oxygen and water vapour, and $\mu_{t,P}^{w(g)}$ is the chemical potential of water which is in equilibrium with water in the electrolyte.

By considering the ideal gas comportment of the wet gases (hydrogen and oxygen) and the gaseous solutions, the chemical potential can be derived as:

$$\mu_{t,P}^{i}=G_{t,P_0}^{i}+RT\ln(P^{i}) \quad (14)$$

where the first term on the right-band is the molar free energy of the pure component as an ideal gas at 1 atm pressure and temperature t, and P^i is its partial pressure in the gaseous solution. Eq. (13) will be written as:

$$nFE_{t,P}^{Rev}=\left(G_{t,P_0}^{H_2}+0.5G_{t,P_0}^{O_2}-G_{t,P_0}^{w(g)}\right)+RT\ln\left(\frac{(P-Pw)^{1.5}}{Pw}\right) \quad (15)$$

By introducing the relation between the free energy of water in gaseous phase and liquid phase (LeRoy and Bowen [20]) and the negative of the standard free energy of formation of liquid water at given temperature. Eq. (15) becomes:

$$nFE_{t,P}^{Rev}=nFE_{t,P_0}^{Rev}+RT\ln\left((P-Pw)^{1.5}\frac{Pw^{*}}{Pw}\right) \quad (16)$$

where

$$nFE_{t,P_0}^{Rev}=\left(G_{t,P_0}^{H_2}+0.5G_{t,P_0}^{O_2}-G_{t,P_0}^{w(l)}\right)=-\Delta G_{ft,P_0}^{w(l)} \quad (17)$$

2.2.3. Temperature effect on reversible potential

The reversible potential is strongly affected by the temperature and the variation can be extracted by introducing a Gibbs–Helmholtz thermodynamic relation between the enthalpy and the Gibbs free energy expressed as [24]:

$$\frac{\partial(G/T)}{\partial T}=-\frac{H}{T^{2}} \quad (18)$$

It follows the relation between the reversible potential and the enthalpic voltage [20]:

$$\frac{\partial\left(E_{t,P_0}^{Rev}/T\right)}{\partial T}=-\frac{V_{t,P_0}^{tp}}{T^{2}} \quad (19)$$

Eq. (19) reveals the impact of the enthalpic voltage correlation on the temperature evolution of reversible potential at atmospheric pressure. After integration of the enthalpic voltage correlation (Eq. (5)) and rearrangement E_{t,P_0}^{Rev} is given by:

$$E_{t,P_0}^{Rev}=1.50342-9.956\times10^{-4}T+2.5\times10^{-7}T^{2} \quad (20)$$

Note that the relative deviation from NIST experimental data doesn't exceed 0.01%. The compared temperature evolution of E_{t,P_0}^{Rev} is presented in Fig. 2 and reveals a good agreement with experimental data extracted from NIST. The expression of the reversible voltage proposed in this work (Eq. (20)) is more accurate and has simplest form (polynomial function) than the conventional correlation proposed by LeRoy [20] which has a relative deviation twice as large as the one proposed in this study (see Fig. 2). The reversible potential at atmospheric

Table 1 – Temperature evolution of virial coefficient.

	B (cm^3/mol)	C (cm^6/mol^2)
H_2	$B=20.5-(1857/T)$	$C=-351+(12{,}760/T^{0.5})$
O_2	$B=42.6-(17{,}400/T)$	$C=-2604+(61{,}457/T^{0.5})$

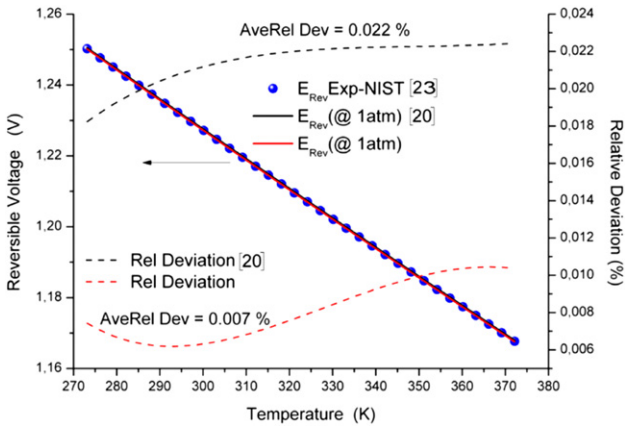

Fig. 2 – Compared temperature evolution of reversible voltage at atmospheric pressure.

pressure decreases with an increasing of temperature and pass from 1.229 V at 298.15 K to 1.167 V at 373.15 K. This finding leads us to promote the increasing of the operating temperature of electrolyzers beyond 100 °C. For this purpose, the use of pressurized electrolyzers will be justified for two reasons; firstly the increasing of boiling temperature of the electrolyte and also obtaining pressurized hydrogen thereby decreasing energy spent during compression process storage. Fig. 3 shows the pressure evolution of the thermoneutral, high heating-value and reversible voltages at different temperatures ranging from 25 °C to 150 °C. The figure reveals a good agreement with precedent work of LeRoy [20] concerning thermoneutral and high heating voltages and reversible voltage providing from Onda [21]. The analysis of the curve reveals that the thermoneutral voltage tends to the high heating-value voltage for large operating pressure and its limit depends on the temperature: 20 bar at $T = 70$ °C and 100 bar at $T = 150$ °C.

2.2.4. *Pressure effect on reversible potential*

The wet gases (hydrogen and oxygen) near the electrode are in contact with gaseous solution of KOH at pressure Pw which

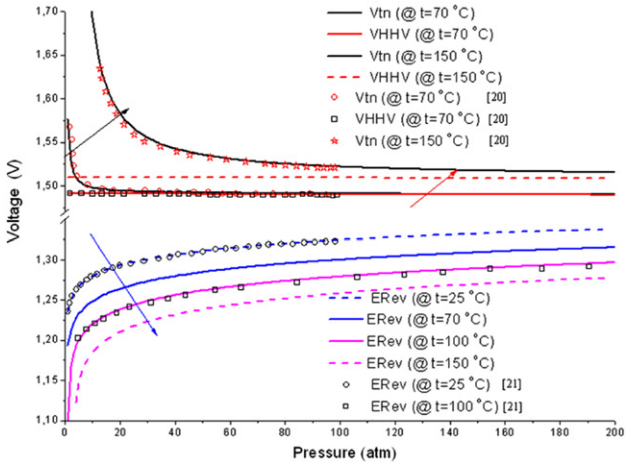

Fig. 3 – Compared pressure evolution of thermodynamic voltage at different temperatures.

can be expressed as a function of the vapour pressure of pure water Pw^* at temperature T and molarity m of the aqueous KOH solution. The most useful correlation was proposed by LeRoy [20] and based on the work of Washburn in International Critical Data, vol. 3 [25].

$$Pw = T^{-3.498}\exp\left(37.93 - \frac{6426.32}{T}\right)\exp \times (0.016214 - 0.13802m + 0.19330\sqrt{m}) \quad (21)$$

$$Pw^* = T^{-3.4159}\exp\left(37.043 - \frac{6275.7}{T}\right) \quad (22)$$

The molarity can be expressed as a function of temperature and concentration of KOH solution Wt% and the proposed correlation is inspired by the experimental study of Gilliam [26].

$$m(t, Wt\%) = \frac{Wt\%(183.1221 - 0.56845T + 984.5679\exp(Wt\%/115.96277))}{100(56.105)} \quad (23)$$

In developing the expressions for the enthalpies voltage and the higher-heating-value voltage, corrections arising as a result of the non ideality of the individual gases were provided and presented previously. Analogous corrections to $E_{t,P}^{Rev}$ can be made and the molar free energy become:

$$nFE_{t,P}^{Rev} = nFE_{t,P_0}^{Rev} + RT\ln\left((P - Pw)^{1.5}\frac{Pw^*}{Pw}\right) + (P - Pw)\left(B^{H_2} + 0.5B^{O_2}\right) + \frac{(P - Pw)^2}{2RT}\left(C^{H_2} + 0.5C^{O_2} - \left(B^{H_2}\right)^2 - 0.5\left(B^{O_2}\right)^2\right) \quad (24a)$$

where B^i and C^i are respectively the 2nd and the 3rd virial coefficient of hydrogen and oxygen gas supposed non ideal while the gaseous solution supposed to be.

By implementing the thermal variation of the virial coefficients the reversible voltage can be expressed as;

$$E_{t,P}^{Rev}/V = E_{t,P_0}^{Rev} + \frac{RT}{nF}\ln\left((P - Pw)^{1.5}\frac{Pw^*}{Pw}\right) + (P - Pw)\left(21.661 \times 10^{-6} - \frac{5.471 \times 10^{-3}}{T}\right) + (P - Pw)^2\left(-\frac{6.289 \times 10^{-6}}{T} + \frac{0.135 \times 10^{-3}}{T^{1.5}} + \frac{2.547 \times 10^{-3}}{T^2} - \frac{0.4825}{T^3}\right) \quad (24b)$$

The reversible voltage variation can be divided into three effects; the most important is the temperature that is taken into account by the first term E_{t,P_0}^{Rev}, calculated at atmospheric pressure. The second term expresses the impact of the pressure and the last two terms express the effect of consideration of real gas on the reversible voltage. Considering real gas instead ideal gas in the estimation of the reversible voltage increase the pressure term (2nd term) by 1.3% and 6.5% at respectively 200 and 700 bar. This implies that the assumption of ideal gas remains valid for operating pressures below 200 bar and small changes in reversible voltage are observed in the range of 1.5–10 mV respectively for 200–700 bar.

Fig. 3 depicts the compared variation of the thermoneutral voltage, high heating voltage and reversible voltage as a function of operating pressure P below 200 atm for different temperatures. In order to compare our approach with ones in the literature [20,21] the figure presents some results at 25, 70, 100 and 150 °C.

Fig. 3 reveals a good agreement with the literature data provided from LeRoy et al. for high heating voltage and thermoneutral voltage while the reversible potential is compared with data provided from the work of Onda et al. [21]. The figure shows that the thermoneutral voltage tends to the high heating voltage for the high operating pressure.

The increasing temperature (from 70 to 150 °C) induced a small growing of the high heating voltage (25 mV) and an increase in thermoneutral voltage depending on the operational pressure (700 mV at 5 atm and 25 mV to 200 atm), whereas we find a decrease in the reversible potential (85 mV at 5 atm and 40 mV to 200 atm).

The increasing of the pressure from 1 atm to 200 atm induces a decrease of thermoneutral voltage equal to 80 mV at 70 °C and 720 mV at 150 °C. The same pressure raising doesn't affect the high heating voltage while we observe the increasing of the reversible voltage equal to 110 mV at 25 °C and 150 mV at 150 °C. These observations permit to predict an increasing of the power consumption of the electrolyzer at high pressure which is in accord with the result of Onda et al. [21].

2.3. *Electrochemical effects*

The rate of the electrode reaction, characterized by the current density, firstly depends on the nature and pretreatment of the electrode surfaces. Secondly, the rate of reaction depends on the composition and concentration of the electrolytic solution adjacent to the electrodes. In a redox reaction, the Gibbs energy of the reaction is proportional to the activation overvoltage in the vicinity of the cathode and anode and can be expressed as: $\Delta G^c = \Delta G_c^{Eq} + \alpha_c nF\eta$ and $\Delta G^a = \Delta G_a^{Eq} - \alpha_a nF\eta$ where $\Delta G_{a/c}^{Eq}$ represent the variation of Gibbs energy at equilibrium and the free energy modified by the overvoltage can be schematized in Fig. 4 as:

The rate constant of a redox reaction K_{Red}, K_{Ox} can be in general expressed by the Arrhenius [27] and written as a function of Gibbs energy variation:

$$K_{Red} = f_{Red}\exp\left(-\Delta G^a/RT\right) = f_{Red}\exp\left(-\Delta G_a^{Eq}/RT\right)\exp\left(\alpha^a nF\eta/RT\right)$$
$$K_{Ox} = f_{Ox}\exp\left(-\Delta G^c/RT\right) = f_{Ox}\exp\left(-\Delta G_c^{Eq}/RT\right)\exp\left(-\alpha^c nF\eta/RT\right) \quad (25)$$

where η is the activation overvoltage and $f_{Red/Ox}$ the frequency factor.

The cell net current is defined as $i = i_{Red} - i_{Ox} - = i_a - i_c$ which every partial current is proportional to the constant rate of the redox reaction, local concentration and electrode surface. Insertion Eq. (25) into net current relation yields the complete current-potential characteristic and known broadly as the Butler–Volmer formulation of electrode kinetics, in honour of the pioneers in this area.

$$i = Fk^0\left(A_{Red}C_{Red}\, e^{\frac{\alpha^a}{RT}nF\eta} - A_{Ox}C_{Ox}\, e^{\frac{-\alpha^c}{RT}nF\eta}\right) \quad (26)$$

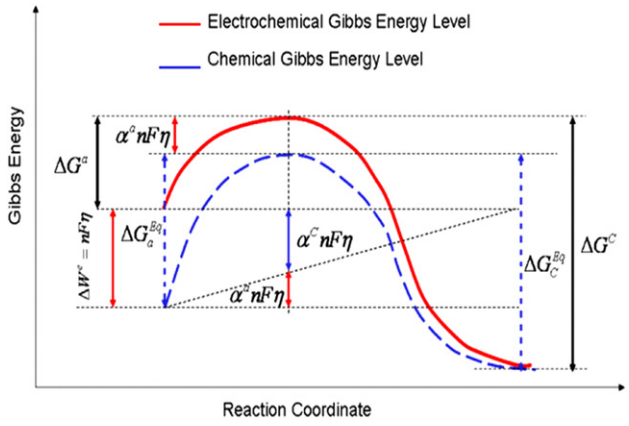

Fig. 4 – Effect of potential change on Gibbs energies: the overall relationship between energy change and state of reaction.

where $A_{Red/Ox}$ the electrode surface area through which the current passes, k^0 is the standard rate constant, $C_{Red/Ox}$ is the concentration of reaction species at the electrode.

The physical parameter k^0 measures the kinetic facility of a Redox couple and reveal the complexity of the system reaction. Equilibrium is achieved on a short time for a large k^0 and sluggish for the smaller ones. The transfer coefficient α or charge-transfer factor is a measure of the symmetry of the energy barrier.

It has been widely accepted that the value of the charge-transfer coefficient, α depends on the rate-determining step (rds) of a multi-step reaction [28] and temperature by linear function as reported from several studies [29–31]. In most systems the value is set between 0.3 and 0.7, and it can usually be approximated by 0.5.

The increasing of potential by η, will induce a decreasing of electrons relative energy by $nF\eta$ as illustrated in Fig. 4. The decrease in turn reduces the Gibbs free energy of the hydrogen ions in the hydrogen evolution reaction by $nF\alpha^a\eta$, while the Gibbs free energy of hydrogen increases by a $nF\alpha^c\eta$.

By introducing the current of the reversible water splitting reaction named as the exchange current $i_0 = Fk^0A_{Red}C_{Red} = Fk^0A_{Ox}C_{Ox}$ [27], thus Butler–Volmer equation can be simplified as:

$$i = i_0\left(e^{\frac{\alpha^a}{RT}nF\eta} - e^{\frac{-\alpha^c}{RT}nF\eta}\right) \quad (27)$$

2.3.1. *Approximate forms of the* $i - \eta$ *equation*

For small values of overvoltage η, the net current is linearly related to overvoltage and the Butler–Volmer equation can be approximated as:

$$i = \frac{j_0A_{Red}nF(\alpha^c + \alpha^a)}{RT}\eta \quad (28)$$

Note that the ratio η/i has units of resistance and is often called the charge-transfer resistance, Rct.

For large values of η $(\eta \geq (RT/nF(\alpha^a + \alpha^c))(4.605 + \ln(A_{Ox}/A_{Red})))$, one of the exponential terms becomes negligible $(A_{Ox}\, e^{(-nF\alpha^c/RT)\eta} \leq 1\%\, A_{Red}\, e^{(nF\alpha^a/RT)\eta})$ and the Tafel logarithmic equation can be used to approximate the Butler–Volmer equation:

$$\eta_{a/c} = -2.3026\frac{RT}{nF\alpha^{a/c}}\,\mathrm{Log}(i_0) + 2.3026\frac{RT}{nF\alpha^{a/c}}\,\mathrm{Log}(i) \quad (29)$$

The Tafel form can be expected to hold whenever the back reaction (i.e., the anodic process, when a net reduction is considered, and vice versa) contributes less than 1% of the current, as mentioned previously.

The linear relationship between the overpotential and the logarithm of current density is characterized by the Tafel slope and exchange current i_0. Both parameters are commonly used as kinetic data to compare electrodes in electrochemistry and depend on the electrolyte concentration and electrode porosity.

As part of this work, the determination of activation overvoltage anodic and cathodic takes into consideration the electrochemical material constituting the electrodes (α, i_0) and also the influence of temperature on each one of them. The correlation used to describe the transfer-charge coefficient for Ni electrode is:

$$\alpha^a = 0.0675 + 0.00095T \quad \text{and}$$
$$\alpha^c = 0.1175 + 0.00095T \quad (r^2 = 0.99887) \quad (30)$$

Fig. 5 shows the comparative evolution of the activation overvoltage on the cathode and the anode for two temperatures 25 and 100 °C. The curves show that the anodic activation overpotential is larger than the cathode overvoltage limiting the reactions of the alkaline electrolysis. The rise in the temperature decreases the activation voltage. Fig. 6 shows the impact of the value of the transfer-charge coefficient at different temperatures and reveal a difference between the activation overpotential calculated by the conventional value ($\alpha^a = \alpha^c = 0.5$) depicted by the dot line and that provided from the temperature correlation depicted by solid line. The relative deviation between these two approaches is inversely proportional to the temperature and pass from 34% to 17% at respectively 25 and 90 °C and for maximum current density value.

2.4. *Two-phase flow effects*

Hydrogen gas is produced within the electrolyte in the vicinity of the electrode. It retains the hydrogen bubble formed until it reaches a critical size enabling it to leave the electrode surface

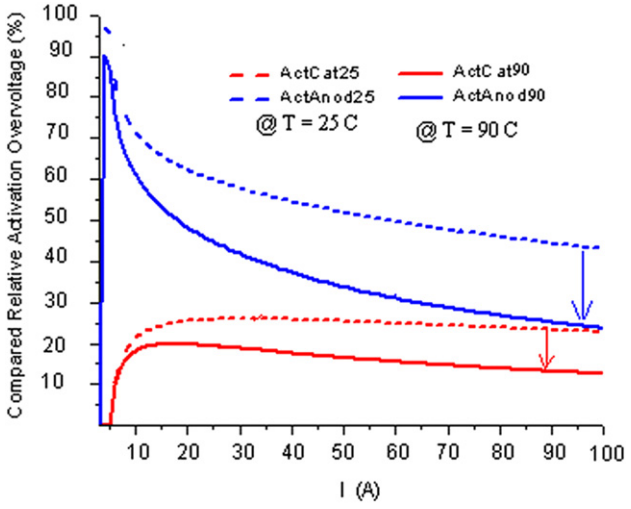

Fig. 5 – Relative activation overvoltage on the cathode and the anode of an alkaline electrolyzer.

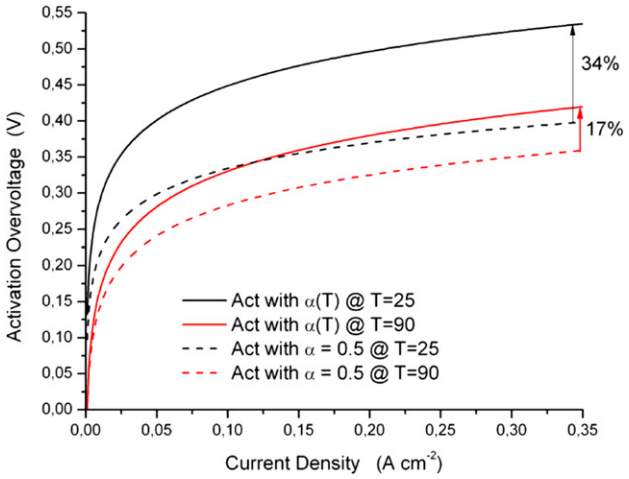

Fig. 6 – Effect of the transfer-charge coefficient on activation overvoltage for different temperatures.

and thereby overcome the resistivity [6]. Thus bubbles produced change the nature of the electrolyte and produce a local movement of the electrolyte. The flow regimes are usually laminar and will be turbulent (wavy two-phase flow). There are two characteristic parameters representing the bubble effect. The first one indicates the bubbling rate (gas voidage fraction) in the bulk electrolyte $\varepsilon = \upsilon_B/\upsilon_T$ and is defining as the relative volume of bubble υ_B according to the volume of electrolyte υ_T. The second one $\vartheta = f(\varepsilon) \equiv (2\varepsilon/3)$ relates the coverage rate of the electrode surface by the bubble curtain and induces a decreasing of effective electrode surface, thus an increasing locally the current density. The complexity of this phenomenon and its impact on the mass transfer coefficient incited numerous studies. A critical review of experimental gas voidage data for gas–liquid mixtures available in the literature yields the result that electrical conductivity of the gas–liquid mixture decrease strongly with respect to the gas voidage fraction. Some of the equations available in the literature are presented, compared by Kreysa and Kuhn [32] and listed in Table 2 revealing that the Maxwell and the Bruggemann equations are mainly recommended as being reliable. Kisdnasamy in 1984 [33] proposes an estimation of the gap resistance induced by the bubbling phenomena and compares experimental data with mathematical function and empirical correlations presented in Fig. 7.

Jansen and Hoogland [34] and Hine and Murakami [35] showed that the recovery rate of the electrode surface by the bubbles decreased by forced convection of electrolyte and that the distribution of bubbles was growing along the electrodes. Vogt [4] reveals that for low current density, the evolution of the bubbles is mainly driven by molecular diffusion. Dahlkild [36] and Mat et al. [37] have shown using the two-phase flow approach that the bubbles distribution was not uniform along the electrode and in the perpendicular direction [38]. At higher current densities gas bubbles nucleated at multiple sites on the electrode developed simultaneously with the gas dissolved in the electrolyte [39]. In this operating condition, the bubbles formed become closer to each other; they interact, meet and merge, preventing contact of the liquid electrolyte

Table 2 – Relative electrical conductivity equations for gas–liquid mixtures.

Relative electrical conductivity	Author
$K_e/K_0 = (1-\varepsilon)/(1+\varepsilon)$	Rayleigh
$K_e/K_0 = (1-\varepsilon)/(1+0.5\varepsilon)$	Maxwel
$K_e/K_0 = 8(1-\varepsilon)\,(2-\varepsilon)/(4+\varepsilon)\,(4-\varepsilon)$	Tobias
$K_e/K_0 = (1-\varepsilon)^{1.5}$	Bruggeman
$K_e/K_0 = 1-1.5\varepsilon+0.5\varepsilon^2$	Prager

with the electrode. Thus, an unstable film of bubbles forms on the electrode surface, which breaks and reforms permanently with low frequency. Generally named as bubble curtain, and induce locally an increase in current density and fluctuating overvoltage around a mean value due to the intermittent nature of the bubble curtains [5–7] and [40].

Fig. 7 reveals a variation of the relative resistance induced by the bubble effect. An increasing of 175% is experimentally observed for $\varepsilon = 0.6$, the mathematical function capture with a good agreement the experimental data produced by Kisdnasamy [33] and the deviations between these various equations are quite small and nearly always less than 10% [32].

2.5. *Geometrical and conceptual effects*

2.5.1. *Effects of electrodes design*

Fouad and Sedahmed [41] and later Elsner in 1984 [42] studied the relationship between gas production and the coefficient of mass transfer to electrodes oriented vertically and horizontally. Jorne and Louvar [43] and Janssen et al. [44] concluded that the electrodes with a three-dimensional texture promote the breakout of hydrogen bubbles produced, thereby decreasing the ohmic resistance of the electrolyte. Similarly, Hine and Murakami [35] and later Albuquerque et al. [45,46] studied the impact of perforated electrode with a specific porosity on the cell overvoltage and the frequency of bubble detachment.

2.5.2. *Effects of electrolyte type and its concentration*

Several studies have shown the impact of the type of electrolyte on the electrolytic cell voltage and thus the performance of the electrolyzer. Investigations revealed both influence of concentration and temperature on the evolution of electrical conductivity (resistivity) of the electrolyte (see Fig. 8) [47,48].

Gilliam [26] showed the existence of a maximum value of electrical conductivity depending on a optimal mass concentration from 30 to 50% and operating temperature. As part of this work, a correlation is proposed to describe the evolution of electrical conductivity as a function of temperature T and the mass concentration wt% based on the experimental work of Klochko and Godneva [49]. See [50] is given as follows and presented in Fig. 9:

$$\begin{aligned}\sigma(w,T) = {} & 2.96396 - 0.02371T - 0.12269w \\ & +(5.7e-5)T^2 + 0.00173w^2 \quad +(4.7e-4)w - (3.6e-8)T^3 \\ & +(2.7e-6)w^3 - (8.9e-6)Tw^2 + (2.4e-7)T^2w \end{aligned} \tag{31}$$

The correlation obtained can estimate the evolution of the electrical conductivity of a solution of KOH in the following ranges $273.15 \le T \le 373.15$ and $10\% \le w \le 45\%$.

The correlation proposed has a good agreement with experimental data and the fit standard error and r^2 coefficient are respectively equal to 0.0131 and 0.9991.

Fig. 10 shows the effect of variation of the electrolyte concentration on the reversible voltage and on the ohmic overpotential for different temperatures ranging from 25 to 75 °C. The variations of the concentration affect greatly the ohmic overpotential and reveal the optimal electrolyte concentration at the vicinity of 30% while it is evident that its influence is less on the reversible voltage. Using electrolyte with concentrations equal to 15% or 45% induces respectively an increasing of ohmic overpotential by 30% and 33% at $T = 25$ °C and 35% and 15% at $T = 75$ °C. Thus, maintaining the electrolyte concentration at its optimal value (30%) is necessary to optimize the electrolysis process.

2.6. *Thermal effects*

The temperature influences differently the electrolyzer's components. One hand it increases the conductivity of the aqueous KOH solution, and that of the membrane [51,52],

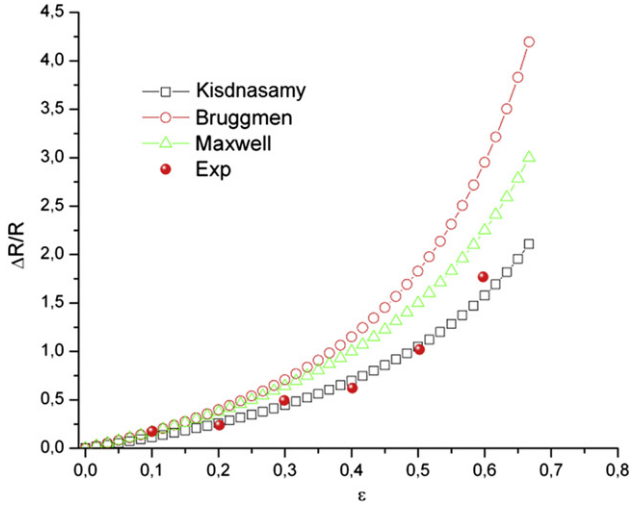

Fig. 7 – Relative variation of the resistance due to the bubbling rate.

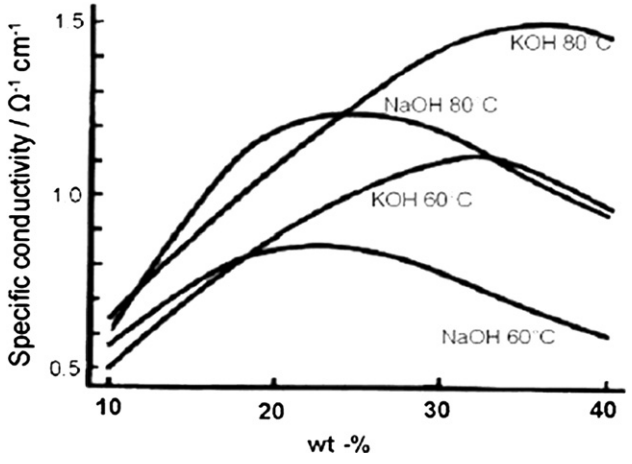

Fig. 8 – Compared specific electrical conductivities of KOH and NaOH electrolyte after Ulmann's encyclopedia of industrial chemistry (2009) [48].

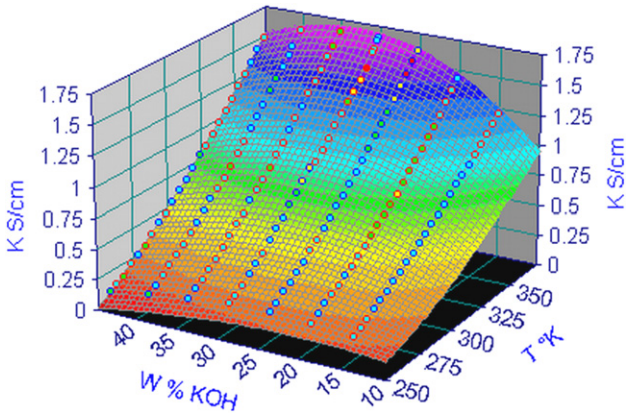

Fig. 9 – Representation of the electrical conductivity of the KOH solution according to concentration and temperature.

while on the other hand decreases the conductivity of the electrodes. The temperature strongly influences the current density of the electrolyzer and thus the production of hydrogen. The impact of temperature on the electrolysis process will be discussed in detail in the following paragraphs.

The temperature of the KOH electrolyte can be determined using thermal model, by assuming a lumped thermal capacitance approach [53], the overall thermal energy balance can be expressed as:

$$C_t \frac{dT}{dt} = \dot{Q}_{gen} - \dot{Q}_{loss} - \dot{Q}_{exch} - \dot{Q}_{cool} \quad (32)$$

where

$$\dot{Q}_{gen} = N_c\left(U - V_{T,P}^{tn}\right) I = N_c\left(U - V_{T,P}^{tn}\right) \frac{JA}{(1-\theta)}$$
$$= N_c\left(U - \left(tn_0(P) + tn_1(P)T + tn_2(P)T^2\right)\right) \frac{JA}{(1-\theta)} \quad (33)$$

$$\dot{Q}_{loss} = \frac{1}{R_t}(T - T_a) \quad (34)$$

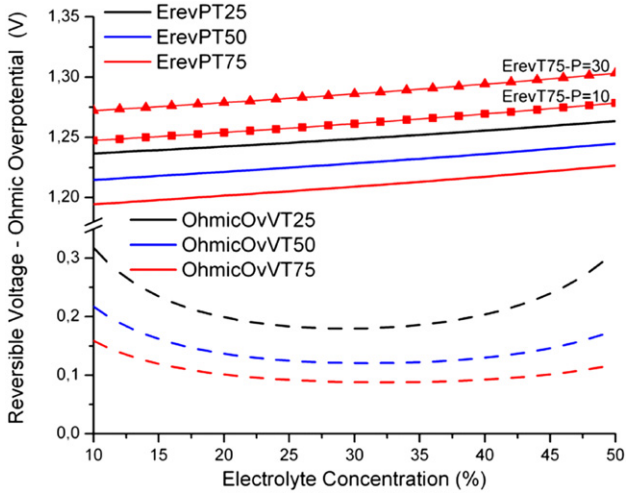

Fig. 10 – Reversible voltage and ohmic overpotential variation according to electrolyte concentration for different temperatures.

$$\dot{Q}_{exch} = \dot{n}_{H_2} C_p^{H_2}(T - T_a) + \dot{n}_{O_2} C_p^{O_2}(T - T_a) + \dot{n}_{H_2O} C_p^{H_2O}(T - T_{in}^w) \quad (35)$$

$$\dot{Q}_{cool} = \dot{m}_f C_p^f \left(T_o^f - T_{in}^f\right) = KS(LMTD) = \dot{m}_f C_p^f \left(1 - e^{-\frac{KS}{\dot{m}_f C_p^f}}\right)\left(T - T_{in}^f\right) \quad (36)$$

$\dot{n}_i$ Represent the molar flow rate of gases and water while $\dot{m}_f$ is the cooling water masse flow rate C_p^f is thermal capacity of fluid at constant pressure. N_c is the number of cells in series per stack and U is the electrolyzer cell voltage.

The first term on the right-hand side of Eq. (32) is the internal heat generation including the variation of thermoneutral voltage in order to take in to account the effect of temperature at low operating pressure and the rate of bubble shadowing the electrodes surface, θ. This last effect increase de local current density and induce more heat generation in the electrolyzer's cell. The thermoneutral voltage $V_{T,P}^{tn}$ can be considering as constant ($V_{T,P}^{tn} = 1.48$ V) [19,54], or can be expressed as a parabolic function of temperature with multiplier constant inversely proportional to the pressure P with relative deviation less than 2% for the temperature up to 80 °C. This assumption permit to introduce the operating pressure as parameter in thermal equation and considering the temperature evolution of the thermoneutral voltage which expression tends to the high heating voltage for pressures above 10 bar for the temperature up to 80 °C. The second term represents the total heat loss to the ambient including heat losses from the gas separator and the stack and can be evaluated thermal resistance Rt. The third term represents the heat exchange with hydrogen, oxygen and reagent water. The forth term represent the auxiliary cooling demand expressed with log mean temperature difference (LMTD). The overall thermal capacity C_t and resistance R_t for the electrolyzer, and the KS-product for the cooling water heat exchanger are the constants that need to be determined analytically or empirically prior to solving the thermal equations with the following assumption $T_{in}^w = T_a$.

Using Eq. (32) as the basis and inserting Eqs. (33)–(36), it can be demonstrated that the overall thermal energy balance on the electrolyzer can be expressed by the linear, first-order, non-homogeneous differential equation in the conventional approach [19] without including the thermal variation of V_{tn} or nonlinear, first-order, non-homogeneous differential equation as proposed in this work. It can be justified by the temperature dependence of the $V_{T,P}^{tn}$ at pressure below 20 bar.

Fig. 11 shows the time evolution of the electrolyte temperature of an alkaline electrolyzer at specific operating conditions. The rising of the electrolyte temperature is due to the Joule effect, induced by the power faded to the electrolyzer. The maximal limit temperature ($T = 80$ °C) is reached after 4.5–5 h (15,000–20,000 s) of operating time. This limit can be reached at different time according to the dimensions and heat capacity transfer performance of the electrolyzer. Fig. 11 reveals that the solution proposed has the same type of evolution as the classical approach, while the influence of the bubble coverage rate is determinant on the rate of variation of the electrolyte temperature. The growing of bubble coverage rate induces an increasing of the current density and thus the dissipative energy by Joule effect.

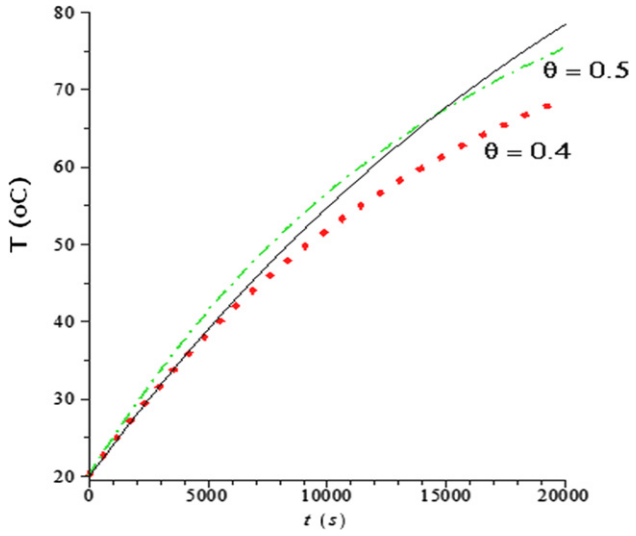

Fig. 11 – Compared temperature evolution of the electrolyzer (solid: conventional approach, solid dot and dot: present work) at P = 25 bar and for the shadowing rate of electrode (θ = 0.4 and θ = 0.5).

$$\frac{dT}{dt} + A_1 T + A_2 T^2 - B = 0 \quad \text{and} \quad T(0) = T_{ini} \tag{37}$$

With analytical solution:

$$T(t) = \frac{-1}{2A_2}\left(A_1 - \sqrt{A_1^2 + 4A_2B}\tanh\left(\sqrt{A_1^2 + 4A_2B}\,\frac{1}{2}\right.\right.$$
$$\left.\left. t + \operatorname{arctanh}\left(\frac{A_1 + 2A_2T_{ini}}{\sqrt{A_1^2 + 4A_2B}}\right)\right)\right) \tag{38}$$

$$A_1 = \frac{1}{C_t}\left(\dot{m}_f C_f\left(1 - e^{-\frac{KS}{\dot{m}_f C_f}}\right) + \frac{1}{R_t} + \dot{n}_w C_p^w + \dot{n}_{H_2}\left(C_p^{H_2} + 0.5C_p^{O_2}\right) + \frac{N_c A J}{(1-\theta)}t_{n1}\right)$$

$$A_2 = \frac{N_c A J}{C_t(1-\theta)}t_{n2}$$

$$B = \frac{1}{C_t}\left(T_{ini}\dot{m}_f C_f\left(1 - e^{-\frac{KS}{\dot{m}_f C}}\right) + T_a\left(\frac{1}{R_t} + \dot{n}_w C_p^w + \dot{n}_{H_2}\left(C_p^{H_2} + 0.5C_p^{O_2}\right)\right) + \frac{N_c A J}{(1-\theta)}(U - t_{n0})\right) \tag{39}$$

The approach adopted in this work takes into account the operating pressure influence on the thermoneutral voltage and thus the heat loss in the electrolyte. This influence is greater at the atmospheric pressure and up to 10 bar as shown in the thermodynamic section. While in the conventional approach adopted up to know [19,54] the solution doesn't take into account the pressure and the bubbling coverage of the electrode which modify the current density by the factor1/(1 − θ).

3. Model development

The set of effects presented in the previous paragraph, is the theoretical basis of multi-physics approach needed to express the cell voltage of an electrolyzer according to the influencing parameters.

3.1. *Multi-physics modelling*

The electrolyzer modelling is essentially based on the cells model and the relationship linking the cells together. In the case where the cells have an equal efficiency, the average model of the electrolyzer can be used by linking the electrolyzer voltage, V_{op}, to the cell voltage, U_c. The cell voltage multiplied by the number of cells, N_c to obtain the electrolyzer's voltage. This approach is the only used today because only the electrolyzer voltage is measured.

The hydrogen production from water by electrolysis, need at least overcome an equilibrium cell voltage, $E_{t,P}^{Rev}$, which is also called "reversible potential". Therefore, even when the equilibrium potential is met, the electrode reactions are inherently slow and then an overpotential ΔU, above the equilibrium cell voltage is necessary in order to kick start the reaction. Overpotential is the deviation of the observed output cell voltage from the thermodynamic reversible cell voltage. The overpotential is generally considered as a kinetic phenomenon and splits into various contributions such as the activation potential of the electrode linked to the slowest of the elementary reaction steps, the rate-determining step (RDS), with the highest kinetic activation barrier. The bubbling overpotentials losses due to the gas phase in the electrolyte and the electrical insulation of the electrode by the bubble attached.

The proposed model is essentially based on the equation of different effects encountered during the process of alkaline electrolysis. Determining the operating voltage across the electrolyzer uses the average model. The latter describes the operating voltage, V_{op}, as the product of the cell voltage, U_c, by the number of electrolyzers' cells, N_c. This approach remains justified as long as we do not have access to the measurement of cells voltage to differentiate their contributions.

The cell voltage can be expressed as a sum of the reversible voltage and all overpotential cited above:

$$U_C = E_{t,P}^{Rev} + (\Delta U_{Act-Mat} + \Delta U_{Act-\theta})_{a/c} + (\Delta U_{Ele-C,T} + \Delta U_{Mem-T} + \Delta U_{Electrod-T}) + (\Delta U_{Ele-\varepsilon}) \tag{40}$$

where:

The activation overvoltage of the electrode providing from the electrochemical reactions includes the effect of recovery rate of the electrode surface, θ, by bubbles.

$$(\Delta U_{Act-Mat} + \Delta U_{Act-\theta})_{a/c} = \frac{2.3026RT}{\alpha^{a/c}nF}\left(\log\frac{i}{i_0^{a/c}} - \log(1-\theta)\right) \tag{41}$$

The linear ohmic overvoltage taking into account the electrolyte, the membrane and the electrode losses, depending on the geometrical aspect of the cell and the electrical conductivities, $K_{T,C}^{i}$ of the materials used.

$$(\Delta U_{Ele-C,T} + \Delta U_{Mem-T} + \Delta U_{Electrode-T}) = \left(\frac{e_{Elect}}{K^{w}_{C,T}A_{Elect}} + \frac{e_{Mem}}{K^{mem}_{T}A_{Mem}} + \frac{e_{Cath}}{K^{Cath}_{T}A_{Cath}} + \frac{e_{Anod}}{K^{Anod}_{T}A_{Anod}}\right)i \quad (42)$$

where e_{Elect}, e_{Mem}, e_{Cath} and e_{Anod} represent respectively the gap between electrode and membrane, the thinness of membrane, cathode and anode.

The overpotential due to the bubbling rate ε in the bulk electrolyte with nonlinear evolution according to the operating current density, j, is modelled as:

$$(\Delta U_{Ele-\varepsilon}) = \frac{e_{Elect}}{K^{w}_{C,T}}\left((1-\varepsilon)^{-1.5} - 1\right)j \quad (43)$$

The increasing of the current density modifies the bubbling rate at the bulk of electrolyte and the rate of electrode coverage. According to the experimental works from Krenz [55], reported by Vogt [7] an empirical correlation was made to describe the bubble rate coverage as a function of current density and temperature.

$$\theta = \left(-97.25 + 182\,T/T_0 - 84\left(T/T_0\right)^2\right)\left(\frac{j}{j_{Lim}}\right)^{0.3} \quad (44)$$

Vogt and Balzer [7] according to the previous work of Piontelli et al. [56] suggests the value of limiting current density as $j_{Lim} = 300\ kA/m^2$.

Note that, for a single bubble layer (with a thickness of two bubble radii) [4] establish the relation between the covering rate bubbling and the bulk bubbling rate as: $\varepsilon = (2/3)\theta$.

3.2. Cell efficiencies

Global energy efficiency is frequently defined as the proportion of the energy output on the total energy input. Depending on how the electrolysis system is assessed and compared, there are three ways of expressing the electrolysis efficiencies: voltaic, faradic and thermal [57,58].

The first efficiency represents the proportion of effective voltage to split water in the total voltage applied to the whole cell and expressed as:

$$\eta_{Voltaic} = \left(\frac{E^{anod} - E^{cath}}{U_c}\right) \quad (45)$$

The Faradic efficiency expresses the Gibbs free energy changes of the water electrolysis reaction such as [57,58]:

$$\eta_{Faradic} = \frac{\Delta G_{t,P}}{nFU_c} = \frac{E^{Rev}_{t,P}}{U_c} \quad (46)$$

The faradic efficiency can be also expressed as the ratio between the actual and theoretical maximum amount of hydrogen produced in the electrolyzer [16,19]. This ratio different from unity can be explained by the parasitic current or in other words by parasitic electrochemical reactions corresponding to multi-steps schemes of water splitting.

The thermal efficiency is usually used and expresses the enthalpy change of water decomposition reaction as the energy input and expressed as:

$$\eta_{Thermal} = \frac{\Delta H_{t,P}}{nFU_c} = \frac{V^{tn}_{t,P}}{U_c} \quad (47)$$

Note that some authors like LeRoy [20], Dau et al. [57] used the high heating voltage in the place of the thermoneutral voltage in order to define the thermal efficiency.

In practice, if the potential drop caused by electrical resistance is 0.85 V at 25 °C and 0.70 V at 70 °C, the following table presents the value of $E^{Rev}_{t,P}$, $V^{tn}_{t,P}$ and their correspondent efficiencies. The thermal and pressure impact on the thermoneutral and reversible voltage and their corresponding efficiencies are presented in Table 3.

The increasing of operating temperature enhances the Thermal efficiency and slightly the Faradic efficiency while the rising of the operating pressure reduce the Thermal and increase slightly the Faradic efficiencies.

4. Validation of the multi-physics model

The multi-physics model was developed and compared with two alkaline electrolyzer's data. The first one is a 5 kW located at the Hydrogen Research Institute (HRI) and is atmospheric with conventional gap (1–2 mm) between the electrode and the membrane. The second one is Phoebus electrolyzer with 26 kW operating power and zero-gap geometry. This last choice is due to its widely used in literature [18,19]. This approach has the dual purpose of comparing the results with experimental data, but also to compare our model with the semi-empirical approaches used up to now.

The characteristic of the electrolyzers studied was summarized in Tables 4 and 5 for respectively HRI electrolyzer and Phoebus electrolyzer.

A Matlab program was developed in order to integrate the different part of the multi-physics model and generate simulation for different operating parameters such as temperature, pressure, concentration and conceptual ones integrating the geometrical aspect and component material specifications.

4.1. Stuart electrolyzer at HRI

The experimental electrolyzer used at HRI was manufactured by Stuart Energy System. It uses alkaline technology Unicell-Cluster™ and operates at atmospheric pressure and temperature range below 80 °C. It produces 1 Nm^3/h of hydrogen and 0.5 Nm^3/h oxygen for a current of 105 A. In the following we present the characteristic current–voltage (U, I) and the thermal efficiency from the multi-physics model compared with corresponding data for different temperatures in the range of 25–53.5 °C, see Figs. 12 and 13.

The curves reveal a good agreement between experimental data and multi-physics model curve developed in this study.

Table 3 – Faradic and thermal efficiencies as function of temperature and pressure.

	@ $T = 25$ °C, $P = 1$ atm	@ $T = 70$ °C, $P = 1$ atm	@ $T = 70$ °C, $P = 30$ atm
$E^{Rev}_{t,P}$ (V)	1.23	1.19	1.27
$\eta_{Faradic}$ (%)	59.13	62.96	64.46
$V^{tn}_{t,P}$ (V)	1.48	1.58	1.49
$\eta_{Thermal}$ (%)	71.15	83.60	75.63

Table 4 – Characteristics of the HRI electrolyzer.

Details of the electrolyzer used in the plant	
Anode	$Ni/Co_3O_4/Fe$ on performed Ni-plate
Cathode	C–Pt on performed Ni-plate
Diaphragms	Ni-mesh supported NiO
Design	1.25 mm spacing
Number of cells	24
Connection	Series
Electrode area	0.03 m^2
Max. current density	3000 A/m^2
Max. block voltage	48–56 V
Max. operation pressure	1 bar
Max. operational temperature	80 °C
Max. power	5 kW
Min. power	0.5 kW
Electrolyte	KOH (30wt.%)

The relative difference between the model and the data does not exceed 0.9%.

4.2. *Phoebus electrolyzer*

The Phoebus electrolyzer is an alkaline type, functioning at $P = 7$ bar and temperature range not exceeding 80 °C. Rated power is 26 kW for a current of 800 A and producing 8 Nm^3/h of hydrogen and 4 Nm^3/h of oxygen [19].

The comparative curves (Figs. 12 and 14) between the simulations obtained from the multi-physics model applied to two different electrolyzers reveal a good agreement with experimental data for all temperatures. Thus, the model can describe with good accuracy different operating conditions and is able to capturing the reality regardless of the electrolyzers' specificities. The simulations require the implementation of structural characteristics of the electrolyzer and its operating conditions to generate the current–voltage curve, the hydrogen production rate and the different efficiencies previously cited. The aim of the comparative study with two different electrolyzers is to demonstrate the versatile character of the model and its ability to be used to simulate the behaviour of electrolyzers. This approach can be provided

Table 5 – Characteristics of the Phoebus electrolyzer.

Details of the electrolyzer used in the plant	
Anode	$Ni/Co_3O_4/Fe$ on performed Ni-plate
Cathode	C–Pt on performed Ni-plate
Diaphragms	Ni-mesh supported NiO
Design	Zero spacing
Number of cells	21
Connection	Series
Electrode area	0.25 m^2
Max. current density	3000 A/m^2
Max. block voltage	35–37 V
Max. operation pressure	7 bar
Max. operational temperature	80 °C
Max. power	26 kW
Min. power	5 kW
Electrolyte	KOH (30–40 wt.%)

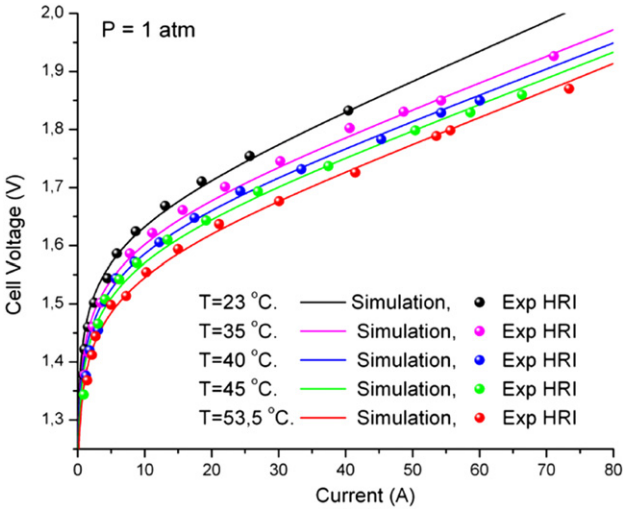

Fig. 12 – Compared simulation of cell voltage with HRI electrolyzer for different temperatures.

in few minutes in comparison with the semi-empirical one requiring few weeks to extract correlations from experimental data [19]. The efficiencies curves providing from simulations have been compared with the efficiencies calculated from experimental data and reveal a good agreement as we can see in Figs. 13 and 15.

4.3. *Model investigation*

4.3.1. *Diagnostic and behaviour analysis by overpotential identification*

Different overvoltages are identified and compared in the multi-physics model. The curves represent the comparative evolution of overpotentials as a function of relative current (i/i_{Max}) for the two studied electrolyzers (HRI and Phoebus).

Fig. 16 shows the evolution of the overpotential obtained respectively with the simulation of the HRI and Phoebus

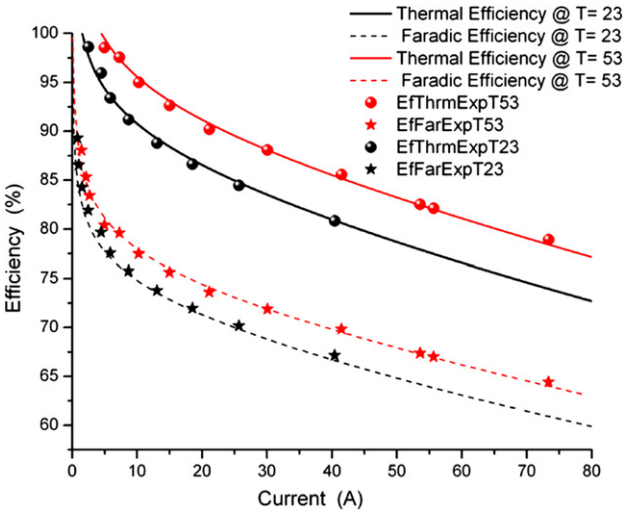

Fig. 13 – Compared thermal efficiency and faradic efficiency for $T = 23$ and $T = 53.5$ °C.

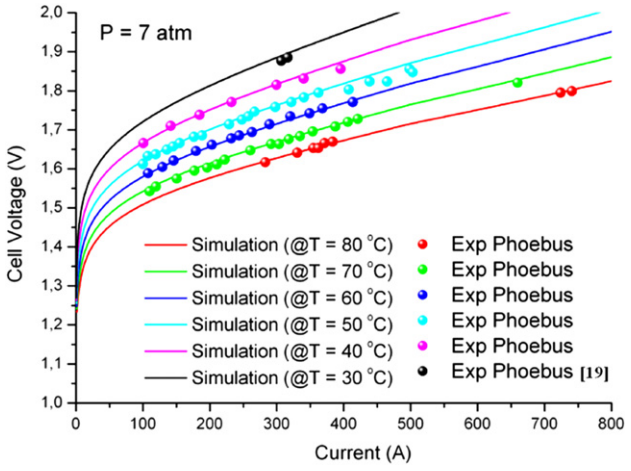

Fig. 14 – Compared simulation with Phoebus electrolyzer cell voltage for different temperatures [19].

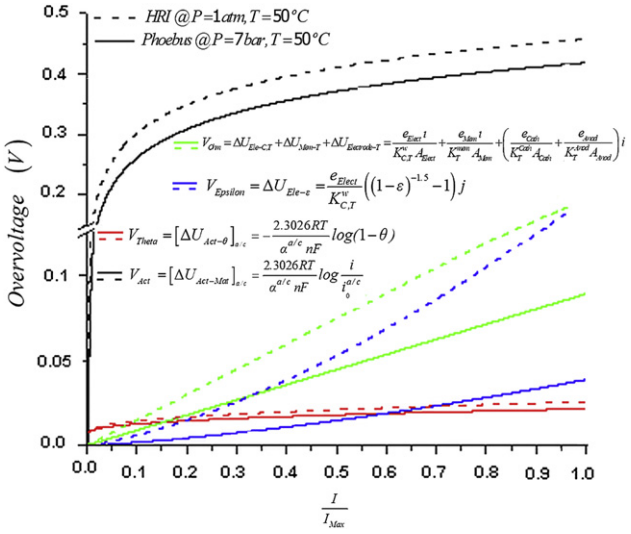

Fig. 16 – Compared overpotential for RHI and Phoebus electrolyzers at T = 50 °C.

electrolyzers. The two curves have identical aspect of the evolution according to the relative current. The compared curves reveal that the activation overpotential is the most important and followed with the same order of importance by the ohmic and bulk bubbling overpotentials. At last the overpotential coming from the shadowing electrode by bubble doesn't exceed few percent. The study shows that overpotentials coming from HRI are larger than the ones providing by Phoebus. This can be explained by the structural consideration (geometrical aspect) in the case of ohmic overpotential and overvoltages due to the bubble in the bulk electrolyte. The geometrical aspect of the two electrolyzers' cells is quite different. The HRI one has conventional aspect while zero-gap aspect is used for the Phoebus electrolyzer. Thus the volume of the electrolyte is smaller and the inherent overvoltage is less important (67% in the case of the ohmic overvoltage and 1/3 for the bulk bubbling overpotential). The activation overvoltages are slightly different (12% in average) because of the nature of the catalyst used in each electrolyzer. Note that the overpotential describing the bubble rate coverage for each electrolyzer is slightly different (16% in average) and can be explained by the difference in the bubbling rate shadowing the electrode surface.

The temperature influences distinctly the different compartments of the electrolyzer and greatly reduces the reversible voltage as shown and losses. Furthermore, the increase in temperature induces an increase of the absorbed current and thus significantly increases twice the amount of hydrogen produced and power absorbed by the electrolyzer.

Fig. 17 shows the effect of temperature on the relative overpotential. The evolution of relative overpotential due to the two-phase flow phenomena (a and c) is proportional to the temperature rising, while the contrary is observed of the electrochemical and ohmic relative overpotentials evolutions (b and d). This last implies that the rising importance of the two-phase flow phenomena when the temperature increasing and thus augment the gas rate production.

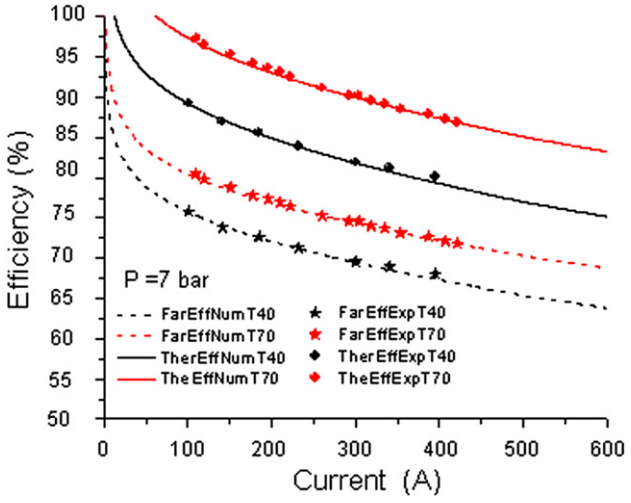

Fig. 15 – Compared thermal efficiency and faradic efficiency for T = 40 and T = 70 °C.

4.3.2. *Temperature and operating pressure influence*

The operating conditions influence significantly the current and power consumed by the electrolyzer. Therefore there estimation allows to predict the normalized hydrogen flow rate which is proportional to current and the power absorbed by the electrolyzer in specific operating conditions.

As shown in Fig. 18, the increasing of temperature induces an increasing of the current and power absorbed. For example an increasing the temperature from 30 °C to 80 °C induces a growing of 57.8% in the current and power absorbed by the electrolyzer, while an increasing of pressure from 1 atm to 70 atm drop the current and power absorbed by 22%.

As shown in Fig. 19(a)–(d), the two electrolyzers behave similarly evolution both in terms of the change in temperature than the operating pressure. The increase in pressure decreases the hydrogen flow rate and the power absorbed by the electrolyzer. The temperature influences both the maximum current i_{T,P_0}^{Max} and maximum power $\dot{W}_{T,P_0}^{Max}$ at $P = 1$ atm but also the decay rate of the power function. The relative

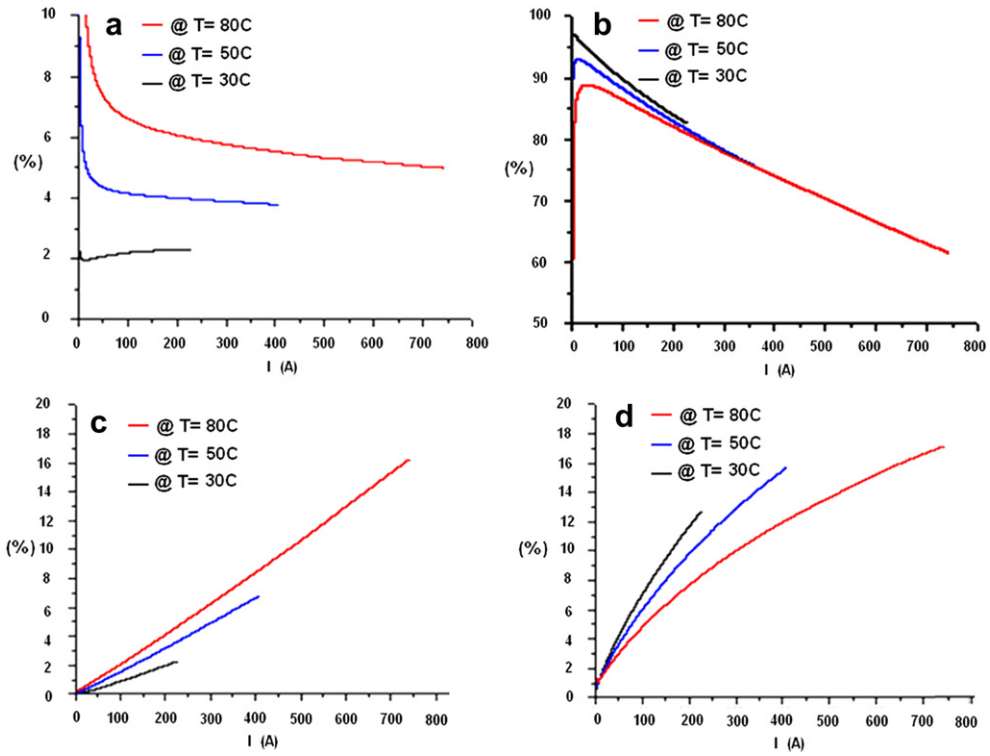

Fig. 17 – Comparative evolution of overpotential according to the current for T = 30, 50 and 80 °C: (a) bubble curtain relative overvoltage, (b) electrochemical activation relative overpotential, (c) bulk bubbling relative overpotential, (d) ohmic relative overvoltage.

variation of the maximum current and maximum power absorbed as a function of the relative operating pressure can be expressed as:

$$\frac{i_{T,P}^{Max}}{i_{T,P_0}^{Max}} = \frac{\dot{W}_{T,P}^{Max}}{\dot{W}_{T,P_0}^{Max}} = \left(\frac{P}{P_o}\right)^{a+bT+cT^2} \tag{48}$$

where the exponent expresses the decay rate and can be correlated with temperature parabolic function and presented in Table 6.

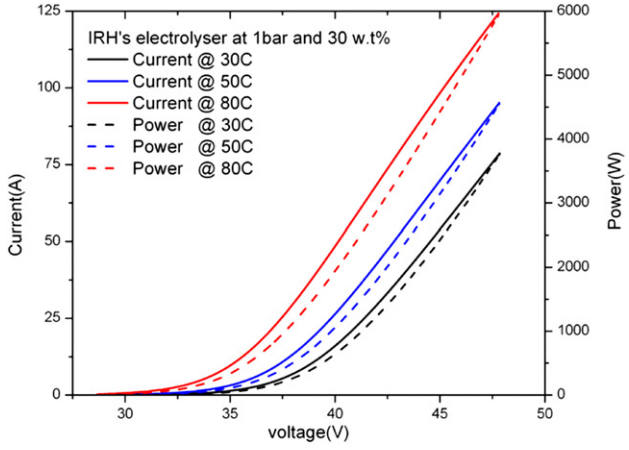

Fig. 18 – Current and power absorbed by the HRI electrolyzer at T = 30, 50 and 80 °C.

The normalized hydrogen flow rate is calculated with the expression:

$$V_{[Nm^3/h]} = \xi_F \frac{3600RT_0}{nFP_0} N_c i \tag{49}$$

ξ_F Represents the current efficiency defines as the ratio between the real amount of hydrogen production and the theoretical estimation.

4.4. *Power consumption using multi-physics model*

In order to compare the power consumption of the electrolysis process under different operating conditions taking into account the auxiliaries equipment. We identify two production processes including atmospheric electrolyzer for the first one and barometric electrolyzer with their auxiliaries at temperature T and pressure P. The first system is constituted by (atmospheric electrolyzer + water pump at 1 atm + solution pump at 1 atm + gas compressor from 1 to P atm) and the second system (barometric electrolyzer at P atm + water pump at P atm + solution pump at P atm). The power consumption of these two processes can be expressed and compared as:

$$\left[\dot{W}_{1,T}^{Ele} + \dot{W}_{1,T}^{w-Pump} + \dot{W}_{1,T}^{sol-Pump} + \dot{W}_{1\to P,T}^{H_2-Comp}\right] \quad \text{and} \quad \left[\dot{W}_{P,T}^{Ele} + \dot{W}_{P,T}^{w-Pump} + \dot{W}_{P,T}^{sol-Pump}\right] \tag{50}$$

The power consumed by the electrolyzer $\dot{W}_{1,T}^{Ele}$ can be calculated by the reversible voltage as mentioned by literature

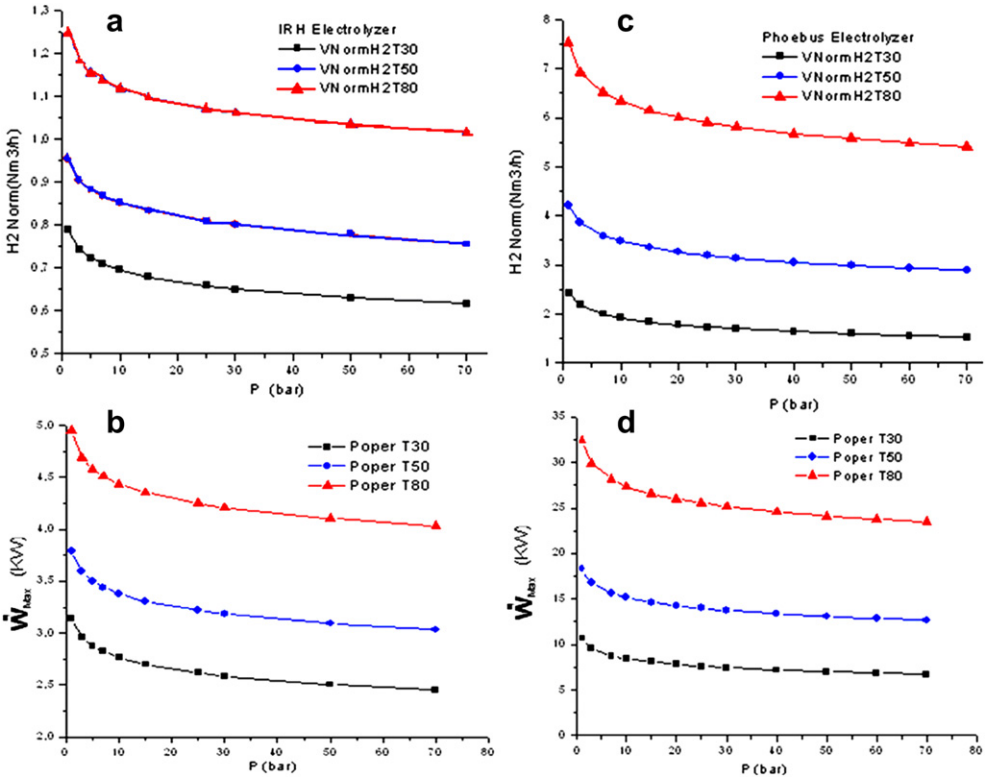

Fig. 19 – Hydrogen flow rate and power absorbed by the RHI/Phoebus electrolyzer as function of operating pressure at $T = 30$, 50 and 80 °C.

[21] but this approach doesn't take into a count the losses induced by the overpotentials. In this work we introduce the effect of the overpotentials to estimate the real power consumption of the electrolyzer for different operating pressure ranging from 1 atm to 100 atm at ($T = 30$,50 and 80 °C). In order to compare the effect of temperature on the power consumption we use a referent current equal to 150 A.

$$\dot{W}_{P,T}^{w/sol-Pump} = \frac{\rho^{w/sol} g h Q^{w/sol}}{\eta^{w/sol-Pump}} = \frac{P^{w/sol} Q^{w/sol}}{\eta^{w/sol-Pump}} \quad (51)$$

is the pump power consumption of the liquid phase, proportional to the fluid flow rate of the reagent water Q^w or recirculation of KOH solution Q^{sol} (500 ml/min).

The power $\dot{W}_{1\to P,T}^{H_2-Comp}$ necessary to compress electrolytic hydrogen was calculated using the following equation (Eq. (52)) where $Q_N^{H_2}$ represents the normalized intake-gas volume flow rate (Nm^3/h) at $P_1^{H_2}$, $P_2^{H_2}$ the discharge pressure (Pa), k the polytropic coefficient ($1 \le k \le 1.4$) with corresponding compressor efficiency η^{Comp}, and Z the compressibility factor depending on the pressure and virial hydrogen coefficients as :

$$\dot{W}_{1\to P,T}^{H_2-Comp} = \frac{1}{\eta^{Comp}} \frac{k}{k-1} P_1^{H_2} \frac{Q_N^{H_2}}{3600} \frac{T_1}{273.15} Z \left[\left(\frac{P_2^{H_2}}{P_1^{H_2}} \right)^{\frac{k-1}{k}} - 1 \right] \quad (52)$$

$$Z = 1 + \frac{B^{H_2}}{RT} P + \frac{\left(C^{H_2} - (B^{H_2})^2 \right)}{(RT)^2} P^2 = 1 + \left(0.247 - \frac{22.336}{T} \right) \frac{P}{T} + \left(-0.112 + \frac{1.846}{T^{0.5}} + \frac{11.015}{T} - \frac{498.889}{T^2} \right) \left(\frac{P}{T} \right)^2 \quad (53)$$

Z represents de deviation between the ideal and real gas considerations and his value depends on the operating pressure P (bar) and temperature T (K).

In this calculation, hydrogen of $T = 303.15$, 323.15 and 353.15 K, $P_1^{H_2} = 1$ atm, $Q_N^{H_2} = 8\ Nm^3/h$, $Q_N^w = Q_N^{H_2}(1 + 1.5Pw/(P - Pw))\ Nm^3/h$, $k = 1.3$, and Z was calculated with Eq. (53) and induces a difference of 0.5 kW at $P = 100$ bar, with a compressor efficiency assumed parametrically to be 25, 50, and 75%.

In this section we focussed our investigation on the temperature impact, compressor efficiency and referent current used to estimate the power consumption of the electrolyzer. The compared study between the two systems of hydrogen production using, in one side the atmospheric electrolyzer and compressor and in the other side barometric electrolyzer and auxiliaries as depicted by Eq. (50) permit to estimate the efficient way to produce hydrogen.

If we consider the power consumption as the product of a referent current (150 A or 700 A) and operating or reversible voltages, the temperature does not change the curves depicting the compared evolution of two systems but only

Table 6 – Coefficient of correlation describing the decay of power consumed by barometric electrolyzer in comparison with the atmospheric one.

Electrolyzer	a	b (k^{-1})	c (k^{-2})
HRI	−0.06711	4×10^{-4}	-2×10^{-6}
Phoebus	−0.1478	17×10^{-4}	1×10^{-5}

inducing a gap in the result. While the compressor efficiency play the main role for determining the best system for hydrogen production and control the atmospheric system production.

Fig. 20 reveals the importance of the compressor efficiency on the estimation of the system based on the atmospheric electrolyzer. The deviation from ideal compressor in the pressure range of 10–30 atm is ranging from 7.9% to 6.3% and 36% to 56.3% for compressor efficiency respectively equal to 0.75 and 0.25. Consider hydrogen as a real gas instead of an ideal gas, induces an increase in the power consumed by the compressor of 5.3% and 10.8% at respectively100 and 200 bar for a temperature of hydrogen stored in 80 °C. These overages are slightly larger gradually as the gas cools. The deviation of the estimation of the atmospheric system considering the ideal gas compression from the real compression doesn't exceed 0.5 kW for $P = 100$ bar. As shown in Fig. 20, the system based on reversible power consumption of the electrolyzer is significantly lower than real power of the electrolyzer and can't be use to compare the two systems. The real power consumed by the electrolyzer depends on the overpotentials and the value of the reference current. This current can be chosen in the range of the maximum current able to be absorbed by the electrolyzer at a given temperature for example 150 A at 30 °C and 700 A at 80 °C. According to this assumption Fig. 20 reveals that the barometric system is more efficient than the atmospheric one. This finding agrees with the work of Onda et al. [21] based on the reversible power consumption of the electrolyzer. The differences between the two hydrogen production systems are significantly larger with this approach (see Table 7) whereas using real power consumption for comparison we see the influence of temperature on the difference between the two systems. At low temperature the difference between the two systems of hydrogen production is ranging from 13.16% to 20.47% for the corresponding ranging pressure between (10–30 bar) while this deviation is ranging from (1.2% and 3%) for operating temperature equal to 80 °C. Thus the atmospheric system production is comparable to the barometric at high operating temperature for operating pressure under 30 bar while at pressure greater than 200 bar, the power consumption of atmospheric system is gaped by 9%.

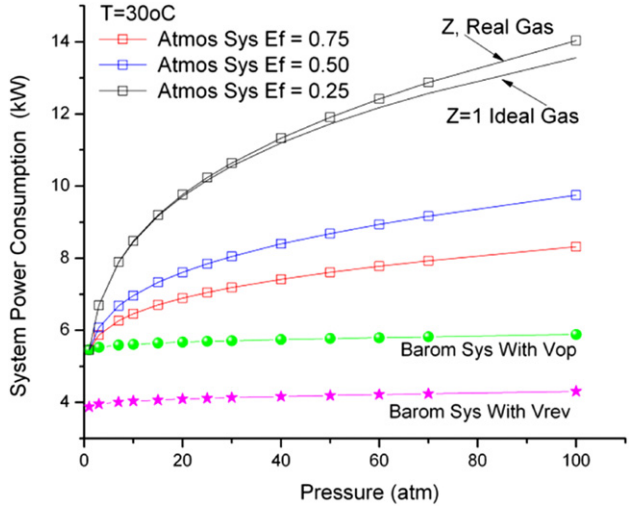

Fig. 20 – Compared system power consumption at T = 30 °C and Iref = 150 A.

Table 7 – Relative difference between two systems of hydrogen production at low and high temperatures.

Temperature	30 °C		80 °C	
Pressure	Rel-dev/ V_{op} (%)	Rel-dev/ V_{Rev} (%)	Rel-dev/ V_{op} (%)	Rel-dev/ V_{Rev} (%)
10	13.16	37.46	1.21	21.05
20	17.71	40.64	2.20	21.66
30	20.47	42.48	3.0	22.14

5. Conclusion

A Multi-physics model describing the evolution of electrolyzer's operating voltage was proposed taking into account geometrical aspect, electrochemical, thermo dynamical and two-phase flow phenomena. This new approach permits to extract the current–voltage characteristic curve using only the electrolyzer's structural parameters in a relatively short time without a large number of experimental data. Comparative studies with experimental data provided from two types of electrolyzer were performed in order to improve the multi-physics model. Results shown to be in good agreement with the experiment, i.e. less than 0.9% relative deviation, for different operating conditions. The implementation of the model in Matlab Simulink program provided conceptual and dimensioning tools and allowed to perform a thermal and barometric study in order to estimate the impact of temperature, concentration of electrolyte and the pressure on the rate and amount of hydrogen production and power consumption of the electrolyzer.

The present thermodynamic study provides a second-order polynomial function expressing the thermal variation of the reversible voltage at atmospheric pressure with relative deviation from NIST experimental data of less than 0.01% thereby improving and simplifying the usual correlation used in literature (LeRoy [20]). The analysis in this work reveals that the thermoneutral voltage tends to the high heating value over operating pressure ranging from 20 to 120 bar at respectively operating temperature of 25 and 80 °C. Thus, replacing $V_{t,P}^{tn}$ by V_{HHV} will not be justified at operating pressures bellow 20 bar. The temperature increase induces a reversible voltage decrease while an increasing of thermoneutral voltage is observed. The pressure increases induces a falling of the thermoneutral voltage and rising of reversible voltage. Thus, the electrolyzer power consumption is enhanced by the temperature but diminished by the operating pressure elevation. Introducing the real gas assumption in the estimation of the thermodynamic potentials induces an increase of the thermoneutral and reversible voltages by 2 mV and 10 mV at respectively 200 and 700 bar. These findings show that the ideal gas assumption is still valid up to 200 bar.

The thermal model used in this investigation permits to take into account the thermal evolution of the thermoneutral

voltage, $V_{t,P}^{tn}$. This approach is necessary for the atmospheric electrolyzers where the V_{tn} depend strongly on temperature while at greater operating pressure $\geq$ 20 bar the V_{tn} tends to the high heating-value voltage V_{HHV} which is considered constant and equal to 1.48 V. In order to obtain an analytical solution of the thermal evolution of the electrolyzer with operating pressure such as parameter, a simplified correlation of V_{tn} is used in this study. This solution allows generalizing and improving the thermal approach of electrolyzer's temperature.

The analysis of the simulation results allows to show the positive impact of temperature on the power consumed by the electrolyzer, the rate of hydrogen production and energy efficiency. It reveals two different aspects of the impact of operating pressure on the electrolyzer and the system for hydrogen production. The increasing of operating pressure induces a decreasing of the power consumed by the electrolyzer and the rate of hydrogen production by a factor depending on the relative pressure and temperature. It increases also the overall energy efficiency by sparing the power consumed in the compression step during the storage of hydrogen. Near the optimal operating temperature of the electrolyzer (80 °C), the two compared systems of hydrogen production consume very similar power (1–3% difference), while at low temperature (T = 30 °C) the gap is larger and varies between 13 and 20% for pressures below 30 bar. The thermal analysis of the two systems of hydrogen production on the basis of the operating voltage shows that the barometric system is globally more efficient than the atmospheric one. Including the overvoltage in the estimation of the power consumption of the two systems of hydrogen production permits to confirm the results of literature [21] based only on the reversible voltage but reveals that the gap between the two approaches decreases with an increasing of temperature and doesn't exceed 6% at 100 bar.

Acknowledgements

This work has been supported by LTE Hydro-Québec, H2CAN Network, Natural Resources Canada and the Natural Sciences and Engineering Research Council of Canada.

REFERENCES

[1] Latrille E, Trably E, Larroche C. Production du Biohydrogène: voie fermentaire sombre. Technique De L'ingénieur, BIO3351; mai 2011.
[2] Ball M, Wietschel M. The hydrogen economy: opportunities and challenges. Cambridge University Press; 2009. Science – 293.
[3] LeRoy RL. Industrial water electrolysis: present and future. International Journal of Hydrogen Energy 1983;8:401–17.
[4] Vogt H. Gas evolving electrodes. In: Yeager E, Bockris JO'M, Convay BE, Sarangapani S, editors. Comprehensive treatise of electrochemistry, vol. 6. New York: Plenum Press; 1983.
[5] Vogt H, Thonstad J. The complex mechanisms inducing anode effects in aluminium electrolysis. In: Schneider W, editor. Light metals 2002. Warrendale: Minerals, Metals & Materials Soc.; 2002. p. 495–501.
[6] Vogt H, Thonstad J. Review of the causes of anode effects. Aluminium 2003;79:98–102.
[7] Vogt H, Balzer RJ. The bubble coverage of gas-evolving electrodes in stagnant electrolytes. Electrochimica Acta 2005; 50(10):2073–9.
[8] Fischer J, Hofmann H, Luft G, Wendt H. Fundamental investigations and electrochemical engineering aspects concerning an advanced concept for alkaline water electrolysis. AIChE Journal 1980;26:794–802.
[9] Yan XL, Hino R. Nuclear hydrogen production handbook. CRC Press Taylor & Francis Group; 2011.
[10] Gutierrez-Martın F, Garcıa-De Marıa JM, Baıri A, Laraqi N. Management strategies for surplus electricity loads using electrolytic hydrogen. International Journal of Hydrogen Energy 2009;34:8468–75.
[11] Gutierrez-Martın F, Confente D, Guerra I. Management of variable electricity loads in wind e hydrogen systems: the case of a Spanish wind farm. International Journal of Hydrogen Energy 2010;35:7329–36.
[12] Takahashi R, Kinoshita H, Murata T, Tamura J, Sugimasa M, Komura A, et al. Output power smoothing and hydrogen production by using variable speed wind generators. IEEE Transactions on Industrial Electronics 2010;57(2).
[13] Korpas M, Greiner CJ. Opportunities for hydrogen production in connection with wind power in weak grids. Renewable Energy 2008;33:1199–208.
[14] Belmokhtar K, Doumbia ML, Agbossou K, Hammoudi M. Hydrogen production from hybrid wind energy system, hydrogen and fuel cells. In: International conference and exhibition, Vancouver (Canada), May 15–18, 2011.
[15] Griesshaber W, Sick F. Simulation of hydrogen–oxygen-systems with PV for the self-sufficient solar house. FhG-ISE, Freiburg im Breisgau; 1991.
[16] Hug W, Bussmann H, Brinner A. Intermittent operation and operation modeling of an alkaline electrolyzer. International Journal of Hydrogen Energy 1993;18(12):973–7.
[17] Havre K, Borg P, Tommerberg K. Modeling and control of pressurized electrolyzer for operation in stand alone power systems. In: Second Nordic symposium on hydrogen and fuel cells for energy storage, Helsinki, January 19–20, 1995. p. 63–78.
[18] Ulleberg O. Stand-alone power systems for the future: optimal design, operation & control of solar-hydrogen energy systems. PhD thesis, Norwegian University of Science and Technology, Trondheim; 1998.
[19] Ulleberg O. Modeling of advanced alkaline electrolyzers: a system simulation approach. International Journal of Hydrogen Energy 2003;28:21–33.
[20] LeRoy RL, Bowen CT. The thermodynamics of aqueous water electrolysis. Journal of the Electrochemical Society 1980:1954–62.
[21] Onda K, Takahiro K, Kikuo K, Hattori K. Prediction of production power for high-pressure hydrogen by high-pressure water electrolysis. Journal of Power Sources 2004;132:64–70.
[22] Roy A, Watson S, Infield D. Comparison of electrical energy efficiency of atmospheric and high-pressure electrolyzers. International Journal of Hydrogen Energy 2006;31:1964–79.
[23] NIST Standard Reference Database. Thermophysical properties of fluid systems, http://webbook.nist.gov/chemistry/fluid/; Oct 2011.
[24] Gaskell DR. Introduction to the thermodynamics of materials. 4th ed. Taylor & Francis; 2003. p. 102.
[25] Washburn EW. International critical tables of numerical data, physics, chemistry and technology, vol. 3. New York: McGraw-Hill; 1928.
[26] Gilliam RJ, Graydon JW, Kirk DW, Thorpe SJ. A review of specific conductivities of potassium hydroxide solutions for

various concentrations and temperatures. International Journal of Hydrogen Energy 2007;32:359–64.
[27] Bard AJ, Faulkner LR. Electrochemical methods fundamentals and applications. 2nd ed. New York: John Wiley & Sons; 2001.
[28] Herraiz-Cardona I, Ortega E, Vazquez-Gomez L, Perez-Herranz V. Electrochemical characterization of a NiCo/Zn cathode for hydrogen generation. International Journal of Hydrogen Energy 2011;36:11578–87.
[29] Conway BE, MacKinnon DJ, Tilak BV. Significance of electrochemical Brønsted factors studies over a wide range of temperatures. Trans Faraday Soc 1970;66.
[30] Conway BE. In: Conway BE, Bockris JO'M, White R, editors. Modern aspects of electrochemistry, vol. 16. New York: Plenum; 1986. p. 103 [chapter 2].
[31] Clouser SJ, Huang JC, Yeager E. Temperature dependence of the Tafel slope for oxygen reduction on platinum in concentrated phosphoric acid. Journal of Applied Electrochemistry 1993;23:597–605.
[32] Kreysa G, Kuhn M. Modeling of gas evolving electrolysis cells: 1. The gas voidage problem. Journal of Applied Electrochemistry 1985;15(4):517–26.
[33] Kisdnasamy S, Neelakantaswamy PS. A quantitative assessment of bubble-curtain effects upon inter-electrode resistance of a conductimetric cell. Journal of Applied Electrochemistry 1984;14:749–54.
[34] Janssen LJJ, Hoogland JG. The effect of electrolytically evolved gas bubbles on the thickness of the diffusion layer. Electrochimica Acta 1970;15:1013.
[35] Hine F, Murakami K. Bubble effects on the solution IR drop in vertical electrolyzer under free and forced convection. Journal of the Electrochemical Society 1980; 127:292–7.
[36] Dahlkild AA. Modeling the two-phase flow and current distribution along a vertical gas-evolving electrode. Journal of Fluid Mechanics 2001;428:249–72.
[37] Mat MD, Aldas K, Ilegbusi OJ. A two-phase flow model for hydrogen evolution in an electrochemical cell. International Journal of Hydrogen Energy 2004;29:1015–23.
[38] Aldas K, Pehlivanoglu N, Mat MD. Numerical and experimental investigation of two-phase flow in an electrochemical cell. International Journal of Hydrogen Energy 2008;33:3668–75.
[39] Eigeldinger J, Vogt H. The bubble coverage of gas-evolving electrodes in a flowing electrolyte. Electrochimica Acta 2000; 45:4449–56.
[40] Wuthrich R, Comninellis Ch, Bleuler H. Bubble evolution on vertical electrodes under extreme current densities. Electrochimica Acta 2005;50:5242–6.
[41] Fouad MG, Sedahmed GH. Mass transfer at horizontal gas-evolving electrodes. Electrochimica Acta 1973;18:55–8.
[42] Elsner C, Coeuret F. Potential distribution along gas evolving electrodes. Journal of Applied Electrochemistry 1985;15(4): 567–74.
[43] Jorne J, Louvar JF. Gas diverting electrodes in the chlor-alkali membrane cell. Journal of Electrochemistry Society 1980;2:127.
[44] Janssen LJJ, Sillen CWMP, Barendrecht E, Stralen SJD. Bubble behaviour during oxygen and hydrogen evolution at transparent electrodes in KOH solution. Electrochimica Acta 1984;29:630–42.
[45] Albuquerque ILT. Influence of cathode geometry on the mass transfer and cathode potential during the water electrolysis in alkaline environment. MsC, Federal University of Campina Grande-PB, Brazil; 2006.
[46] Albuquerque ILT, Cavalcanti EB, Vilar EO. Mass transfer study of electrochemical processes with gas production. Chemical Engineering and Process: Process Intensification 2009;48:1432–6.
[47] Bagotsky VS. Fundamentals of chemical chemistry. A John Wiley & Sons, INC., Pub; 2006.
[48] Ulmann F, Bohnet M. Ullmann's encyclopedia of industrial chemistry. Weinheim, Germany/New York: Wiley-VCH/J. Wiley & Sons; 2009.
[49] Klochko MA, Godneva MM. Electrical conductivity and viscosity of aqueous solutions of NaOH and KOH. Journal of Inorganic Chemistry (USSR) 1959;4:964–8.
[50] See DM, White RE. Temperature and concentration dependence of the specific conductivity of concentrated solutions of potassium hydroxide. Journal of Chemical and Engineering Data 1997;42:1266–8.
[51] Montoneri E. Evaluation of asbestos composite separators in advanced water test electrolyzers. Journal of Applied Electrochemistry 1988;18:280–7.
[52] Vermeiren Ph, Adriansens W, Moreels JP, Leysen R. Evaluation of the Zirfon(R) separator for use in alkaline water electrolysis and Ni-H_2 batteries. International Journal of Hydrogen Energy 1998;23(5):321–4.
[53] Incropera FP, DeWitt DP. Fundamentals of heat and mass transfer. 3rd ed. New York: Wiley; 1990.
[54] Diéguez PM, Ursúa A, Sanchis P, Sopena C, Guelbenzu E, Gandía LM. Thermal performance of a commercial alkaline water electrolyzer: experimental study and mathematical modeling. International Journal of Hydrogen Energy 2008; 33(24):7338–54.
[55] Krenz M. Untersuchung des elektrodennahen Raumes gasentwickelnder Elektroden. Dissertation A, Humboldt-Universitat, Berlin; 1984.
[56] Piontelli R, Mazza B, Pedeferri P, Tognoni A. Ricerchesullosviluppoelettrodico di gas e suglieffettianomalicheloaccompagnano, Sviluppo da soluzioneacquose. Electrochim Metall 1967;2:257–87.
[57] Dau H, Limberg C, Reier T, Risch M, Roggan S, Strasser P, Dau H, Limberg C, Strasser P, et al. The mechanism of water oxidation: from electrolysis via homogeneous to biological catalysis. ChemCatChem 2010;2:724–61.
[58] Zeng K, Zhang DK. Recent progress in alkaline water electrolysis for hydrogen production and applications. Progress in Energy and Combustion Science 2010;36:307–26.